Sedimentologika

Research article

Integrating chemostratigraphy and sedimentology for sequence stratigraphy in an enigmatic Middle to Late Devonian mudstone

Maya T. LaGrange[1], Brette S. Harris[1], Sara K. Biddle[1], Smriti Dhiman[1], Octavian Catuneanu[1], Kurt O. Konhauser[1], Viktor Terlaky[2], Murray K. Gingras[1]

[1] Department of Earth and Atmospheric Sciences, University of Alberta, 1-26 Earth Sciences Building, Edmonton, AB T6G 2E3, Canada
[2] Northwest Territories Geological Survey, 4601 52nd Ave, Yellowknife, NT X1A 1K3, Canada

*corresponding author: Maya T. LaGrange (maya.lagrange@yale.edu)

doi: 10.57035/journals/sdk.2025.e31.1695

Editors: Stéphane Bodin and Abosede Abubakre
Reviewers: Dario Harazim and one anoymous reviewer
Copyediting, layout and production: Jarred C. LLyod, Tom Dodd and Romain Vaucher

Submitted: 21.10.2024
Accepted: 31.07.2025
Published: 03.11.2025

Abstract | Sequence stratigraphy in fine-grained successions is often challenging with traditional datasets, and in such intervals, chemostratigraphy is increasingly used to facilitate interpretations. In this study, we present an example from mudstone units of the Horn River Group (Northwest Territories, Canada), which provide a local record of Middle to Late Devonian marine conditions. The dataset comprises geochemical composition data from X-ray fluorescence (XRF), mineralogical data from X-ray diffraction (XRD), wireline logs, total organic carbon (TOC) profiles, and lithological core and thin section descriptions. We first focus on a mudstone core with high-resolution thin-section and geochemical results, enabling the evaluation of chemostratigraphic signatures associated with surfaces and systems tracts in the Horn River Group. By employing chemostratigraphic proxies for terrigenous sediment supply and proportion of biogenic silica, sequence stratigraphic analysis is extended to three cores and five outcrops lacking extensive thin section coverage. Six complete transgressive–regressive (T–R) sequences are identified and correlated in the Horn River Group, comprising higher-resolution cycles in relative sea-level and sediment supply, which are superimposed on previously identified larger-scale sequences. The sequence stratigraphic framework presented illustrates the local balance between relative sea-level rise and sediment supply along the northwestern margin of Laurentia during the Eifelian to the Frasnian. Moreover, this study demonstrates the utility of integrating chemostratigraphic proxies with sedimentological results as a means of sequence stratigraphic interpretation and correlation in mudstone intervals.

Lay summary | In this study, we look at mudstones from the Horn River Group in Canada, which provide a snapshot of ocean conditions along the ancient North American coast approximately 385 to 372 million years ago. By combining detailed observations with chemical data from rock samples, we interpret how relative sea level and sediment supply changed over time as this rock unit formed. We first focus on one location that has a high-resolution dataset and use the results from this location to guide interpretations in other areas. Our findings reveal six cycles of sea-level rise and sediment supply variation. This study shows how combining detailed observations with chemical data allows us to better understand the history of ancient ocean basins and predict the subsurface distribution of mudstone deposits with economic potential.

Keywords: Sequence stratigraphy; Chemostratigraphy; Black shale; Organic-rich mudstone; Devonian

1. Introduction

Sequence stratigraphy is essential for interpreting changes in sedimentary environments over time and mapping facies distributions in predictive resource exploration. Yet, geological successions dominated by mudstone often present a challenge for those attempting to establish a sequence stratigraphic framework. Such intervals are commonly marked by subtle sedimentological variations relative to coarser-grained clastic and carbonate strata, making it difficult to identify useful lithological trends from outcrop, core, or well logs without a high-resolution

thin section dataset (e.g., Biddle et al., 2021; Egenhoff & Fishman, 2013; Knapp et al., 2017; Macquaker et al., 2007; Pellegrini et al., 2023; Plint, 2014). Moreover, seismic profiles may be nonexistent or lack the stratal geometries useful for sequence stratigraphic interpretations, and in detailed studies of mudstone units, the scale of analysis is generally higher resolution than seismic information allows. Biostratigraphic datasets may also be of limited use in mudstone units: at times because of thermal degradation or the nature of the depositional environment (Ratcliffe et al., 2012b), and for Paleozoic or older strata, due to a lower abundance of datable fossils compared to younger rocks (Eide, 2005; Slatt & Rodriguez, 2012). As with seismic, the resolution of biostratigraphic data may also be insufficient, and the availability of biostratigraphic results can at times be even more limited than the resolution of seismic profiles. Nonetheless, mudstone strata hold an extensive record of Earth's history and past climate-sea level interactions, in addition to providing essential resources in the form of hydrocarbons, industrial raw materials, mineral deposits, and rare earth elements necessary for the energy transition (Biddle et al., 2025; Lazar et al., 2015; Potter et al., 2005; Schieber & Zimmerle, 1998). Owing to the difficulties associated with mudstone stratigraphy, geochemical profiles are increasingly used to facilitate correlations and supplement traditional datasets for high-resolution sequence stratigraphic analyses (e.g., B. S. Harris et al., 2021; Li et al., 2021; Milad et al., 2020; Sano et al., 2013; Thöle et al., 2020; Turner et al., 2016; Wang et al., 2022).

Chemostratigraphy (i.e., chemical stratigraphy) characterizes and correlates sedimentary strata using the geochemical signatures of whole-rock samples (Pearce et al., 1999). For mudstones, geochemical proxies most often take the form of elemental abundance or ratios and have been introduced to analyse a wide range of paleoenvironmental conditions including paleoredox (e.g., Calvert & Pedersen, 1993), basin restriction (e.g., Algeo & Lyons, 2006), detrital sediment flux (Pearce et al., 2005), biogenic silica input (e.g., Arsairai et al., 2016; Davis et al., 1999), and salinity (e.g., Wei & Algeo, 2020). Temporal shifts in a geochemical proxy can be valuable to sequence stratigraphy because the controlling factors (e.g., terrigenous sediment input, paleoredox, degree of basin restriction, or proportion of biogenic silica) are often linked to the balance between relative sea-level change and sediment supply in a sedimentary basin (e.g., B. S. Harris et al., 2021; Turner et al., 2016). There are also several advantages of chemostratigraphic data, most notably: (1) when a core is not available or an outcrop is highly fissile, geochemical results can be acquired from drill cuttings or fissile outcrop samples, (2) the dataset can be collected with non-destructive techniques, such as X-ray Fluorescence, and (3) collecting chemostratigraphic datasets can be time and cost effective.

Limitations exist when employing geochemical datasets in sequence stratigraphic analysis. For instance, the chemostratigraphic signatures of the basal surface of forced regression and correlative conformity (surfaces needed to distinguish normal regression from forced regression) remain unconstrained (sensu LaGrange et al., 2020). Additionally, the elements employed as proxies are influenced by a multitude of environmental and diagenetic factors, which can lead to skepticism that a given proxy reflects transgressive–regressive trends. Many authors have thus emphasized the importance of combining chemostratigraphic results with other available datasets (e.g., petrographical or mineralogical) and using statistical analyses to better constrain element affinities (e.g., Algeo et al., 2004; Hammes & Frébourg, 2012; Ver Straeten et al., 2011; Wesenlund et al., 2022).

This study evaluates the effectiveness of geochemical datasets in sequence stratigraphy by comparing chemostratigraphic profiles with stratigraphic interpretations based on sedimentological data. We focus on a mudstone core with high-resolution thin-section and geochemical data, enabling the assessment of chemostratigraphic signatures of surfaces and systems tracts. The chemostratigraphic framework is then applied to extend sequence stratigraphic analysis to five outcrops and three additional cores lacking extensive thin-section results. The dataset consists of cores and outcrops from the Devonian Horn River Group of the west-central Northwest Territories (NWT), Canada, and includes lithological core and thin section descriptions, wireline gamma-ray and resistivity logs, total organic carbon (TOC), mineralogical composition through X-ray diffraction (XRD) and geochemical composition from X-ray fluorescence (XRF). Biddle et al. (2021) presented sedimentological and ichnological datasets at the thin section scale, which were used to interpret environmental conditions and depositional processes associated with the Horn River Group mudstones. Here, we combine the petrographic depositional interpretations from Biddle et al. (2021) with macro-scale sedimentological observations and chemostratigraphic profiles. The Horn River Group of the NWT comprises mudstone units (Hare Indian and Canol Formations) with coeval platform and reef carbonate units of the Ramparts Formation (Figure 1; Pugh, 1983). The current study focuses on locations where the reef units of the Horn River Group are absent and the mudstone intervals are thicker (Figure 1). This work includes the previously published geochemical dataset from the Hare Indian Formation by Harris et al. (2021), combined with new chemostratigraphic results from the Ramparts, Canol, and Imperial Formations. Through this study, we evaluate the strengths and limitations of geochemical results in sequence stratigraphy.

2. Geological background

2.1. Lithostratigraphy and depositional systems

The strata of the Horn River Group in the west-central NWT were deposited during the late Eifelian to Frasnian of the Middle to Late Devonian (Kabanov & Gouwy, 2017)

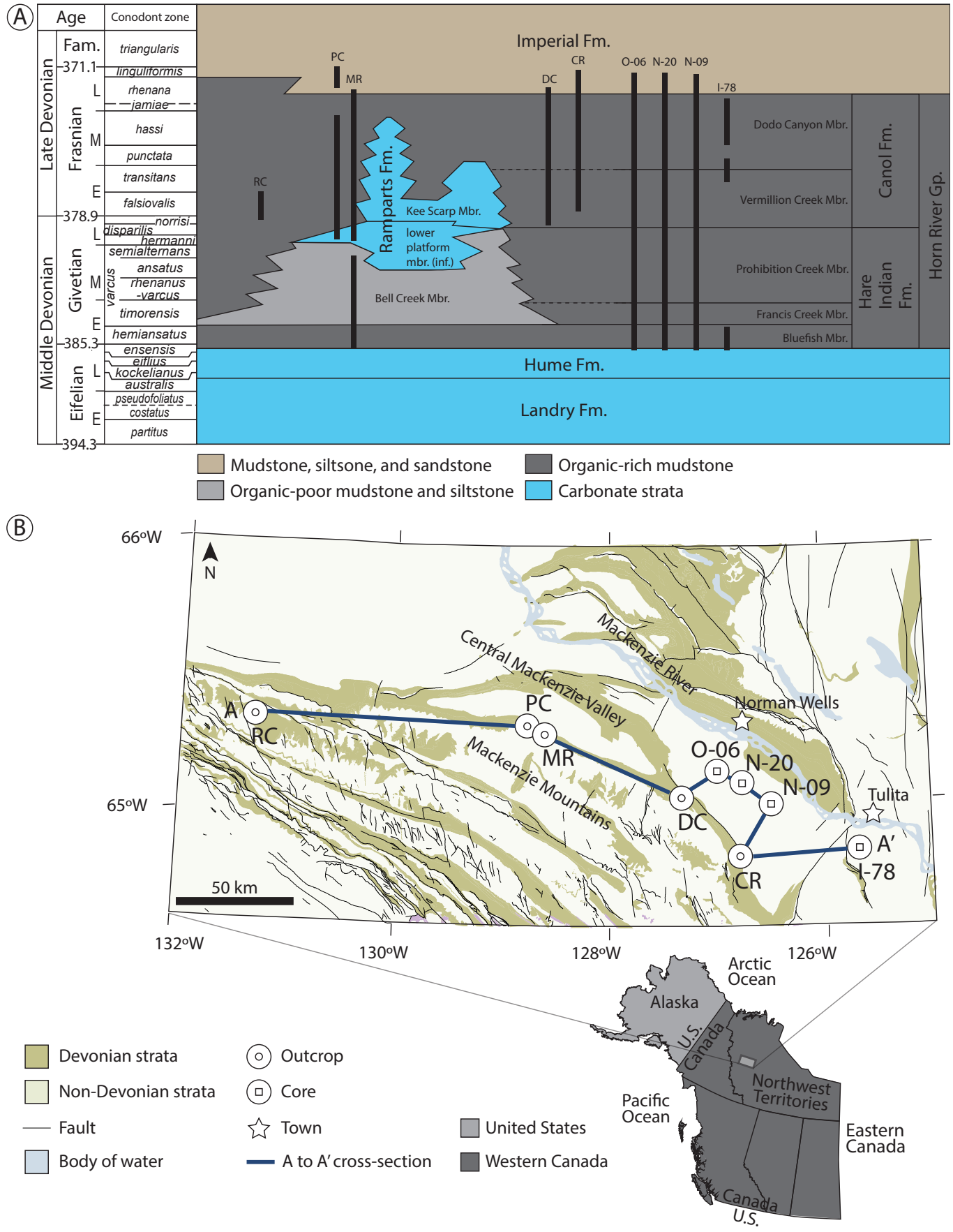

Figure 1 | (A) Schematic stratigraphic column for the Horn River Group in the Central Mackenzie Valley and Mackenzie Mountains of the Northwest Territories (NWT). This chart is modified from LaGrange et al. (2023) after Kabanov and Deblonde (2019) and adjusted to the most recent stage boundary calibrations from Becker et al. (2020). The Francis Creek, Prohibition Creek, Vermillion Creek, and Dodo Canyon Members are defined for the Central Mackenzie Valley but have not been established in the Mackenzie Mountains. The black bars show the stratigraphic position and coverage of the cores and outcrops of this study. Lateral spacing of cores and outcrops is not to scale. (B) Geological map of the study area, showing the locations of cores and outcrops in the Central Mackenzie Valley and Mackenzie Mountains of the Northwest Territories (NWT), Canada. The cross-section line A to A′ is also indicated. Modified from Irwin (2020). Outcrop abbreviations: CR – Carcajou River, DC – Dodo Creek, MR – Mountain River, PC – Powell Creek, and RC – Rumbly Creek. Other acronyms and abbreviations: Fam. – Famennian, Fm. – formation, Gp. – group, Mbr. – member, inf. – informal.

and comprise the Hare Indian, Ramparts, and Canol Formations (Figure 1A). The Horn River Group overlies the Hume Formation and is overlain by the Imperial Formation. In areas where the Ramparts Formation is present, the Hare Indian Formation includes the Bluefish Member, an organic-rich mudstone unit (Pugh, 1983), and the Bell Creek Member, which is characterized by organic-poor mudstone with limestone and siltstone interbeds (Pyle & Gal, 2016). Where the Ramparts Formation is absent, the Hare Indian Formation of the Central Mackenzie Valley includes three Members: the Bluefish, Francis Creek (fissile, argillaceous mudstone), and Prohibition Creek (organic-rich mudstone) (Kabanov & Gouwy, 2017; Pugh, 1983). Moreover, at locations where the Ramparts Formation was not deposited, the organic-rich mudstones of the Canol Formation are subdivided into the Vermillion Creek Member and the Dodo Canyon Member, distinguished by a higher proportion of calcareous mudstone intervals in the Vermillion Creek Member (Kabanov & Gouwy, 2017). The Francis Creek, Prohibition Creek, Vermillion Creek, and Dodo Canyon Members of the Hare Indian and Canol Formations are not distinguished in the Mackenzie Mountains (Figure 1).

Overall, the mudstone units of the Horn River Group are interpreted as a proximal to distal shelf depositional system (Biddle et al., 2021), with the Bell Creek Member possibly representing the distal portion of a delta (Biddle et al., 2021; Tassonyi, 1969). The Ramparts Formation is present where the Bell Creek Member is thickest and comprises limestone and calcareous mudstone ramp and platform deposits, with localized reef units of the Kee Scarp Member (Muir et al., 1985). Above the Horn River Group, the Imperial Formation comprises a basal 10 to 15 m thick mudstone overlain by intercalated sandstone, siltstone and mudstone units and is interpreted as a prograding submarine fan to slope clinoform system (Hadlari et al., 2009). This study includes stratigraphic analysis of the basal Imperial Formation mudstone.

2.2. Tectonic setting

In the Middle to Late Devonian, the study area was located along the northwestern margin of Laurentia, at tropical latitudes near the paleoequator (e.g., Cocks & Torsvik, 2011; Scotese & McKerrow, 1990). Following supercontinent breakup in the Neoproterozoic, a passive margin developed along the present-day northwest margin of Ancestral North America, with convergence to the north (Dewing et al., 2019; Hadlari et al., 2014) and strata of the Horn River Group were deposited in an intrashelf basin along the passive margin. In the Late Devonian, the Ellesmerian orogeny along the northern margin of Laurentia produced a foreland basin in the study area, causing a shift from the organic-rich mudstones and carbonates of the Horn River Group to deposition of the Imperial Formation siliciclastics (Beranek et al., 2010; Garzione et al., 1997). Next, a regional sub-Cretaceous unconformity was produced by uplift and cooling associated with basin inversion. This was followed by renewed burial and then eventual exposure of the Horn River Group strata in the Mackenzie Mountains during development of the North American Cordillera Foreland Basin (Powell et al., 2020). The study area is currently experiencing compression produced by the accretion of the Yakutat terrane onto the North American Craton in the Gulf of Alaska, which began in the Miocene (Mazzotti & Hyndman, 2002).

2.3. Sequence stratigraphy

Initial studies of the Horn River Group focused on the Kee Scarp Reef Member of the Rampart Formation, placing these reef strata in the context of two large-scale sequence stratigraphic cycles (e.g., Muir et al., 1985). The Horn River Group has also been included in a broad-scale sequence stratigraphic framework for the Devonian of the entire Northern Canadian Mainland Sedimentary Basin, where the Horn River Group and surrounding formations are part of two transgressive–regressive (T–R) cycles (Morrow, 2018). Broadly, the two cycles of Muir and Morrow are as follows: (1) Hume Formation to Hare Indian Formation or lower Ramparts Formation, (2) Hare Indian Formation or lower Ramparts Formation to Imperial Formation (Morrow, 2018; Muir et al., 1985), although specific details about the proposed boundaries between the transgressive and regressive portion of the cycles are limited. Using lithofacies interpretations and well-log datasets, Potma et al. (2022) interpreted a depositional sequence largely consistent with the second cycle above, spanning the upper Ramparts Formation to the lowermost Imperial Formation. At locations where the carbonate units are thick and the overlying Canol Formation mudstone unit is thin, higher-frequency cycles were identified in carbonates of the Ramparts Formation, in the form of alternating transgressive systems tracts and highstand systems tracts (e.g., Muir et al., 1985; Muir & Dixon, 1984) or in the form of parasequences (Yose et al., 2001). Moreover, a chemostratigraphy-based sequence stratigraphic framework for the Hare Indian Formation (the lowermost unit of the Horn River Group) was presented by Harris et al. (2021). High-frequency stratigraphic cycles have not previously been identified and correlated in the organic-rich mudstone units of the Canol Formation or the Horn River Group as a whole.

3. Samples and analytical methods

3.1. Cores and outcrops

This study focuses on four cores in the Central Mackenzie Valley of the NWT and five outcrops in the adjacent Shúhta (Mackenzie Mountains), located on the traditional lands of the Sahtu Dene (Figure 1; Appendix A). The four cores are from (1) the MGM Shell East Mackay I-78 well (hereafter referred to as the I-78 core), (2) the Husky Little Bear N-09 well (N-09 core), (3) the ConocoPhillips Mirror Lake N-20 (N-20 core), and (4) the ConocoPhillips Loon Creek O-06 well (O-06 core). The five outcrops are located

along the banks of Carcajou River, Dodo Creek, Mountain River, Powell Creek, and Rumbly Creek, respectively and will be referred to according to those geographical names (Figure 1). Figure 1A illustrates the stratigraphic position and coverage of the cores and outcrops included in this study.

3.2. Sedimentology

In this study, mudstone nomenclature follows the scheme presented in Lazar et al. (2015): fine-grained sedimentary rocks are named by grain size, and modifiers are applied to describe characteristics such as bedding, composition, fossil or trace fossil content, and colour. All cores were described with observations focusing on lithology, bedding, sedimentary structures, fossils, trace fossils, fissility, and composition, with core colour described following the Munsell Geological Rock-Color Chart (Munsell Color, 2009). The core observations were then synthesized to produce lithofacies, and XRD data were used to characterize the mineralogy of each facies (see Section 3.3 for XRD methods).

A petrographic dataset from mudstone units of the Horn River Group was previously described and interpreted in Biddle et al. (2021). For the present study, four new thin sections from the N-09 core were prepared from lithofacies that, until now, did not have any associated thin sections (i.e., lithofacies 1 and 2). Methods for thin section analysis and the interpretation of microfacies, which comprise the microscopic characteristics of rocks (Brown, 1943), can be found in Biddle et al. (2021). Using sedimentological and ichnological results from thin sections, Biddle et al. (2021) previously interpreted environmental conditions and sediment transport processes associated with the Horn River Group mudstones. These depositional interpretations were first presented in Biddle et al. (2021) and are again summarized in Appendix A. The distribution of microfacies with depth was not included in Biddle et al. (2021) and is presented for the first time in this study. Moreover, macro-scale lithofacies were not published in Biddle et al. (2021) and are incorporated herein to extend depositional interpretations from wells with high thin section coverage to wells with low thin section availability (or an absence of thin sections, entirely). In the present work, we integrate for the first time petrographic interpretations with macro-scale lithofacies results and geochemical profiles from the Horn River Group.

3.3. Composition

TOC data were collected with a LECO Analyser by Weatherford Laboratories for the I-78 and N-20 cores and by Core Laboratories Canada for the N-09 core. The mineralogical composition of the four cores was assessed through XRD. The XRD datasets from the N-09, N-20, and O-06 cores were collected by Core Laboratories Canada, whereas the XRD dataset from the I-78 core is from Weatherford Laboratories. Methods for XRD analysis comprised sample pulverization, packing into aluminum sample holders, and analysis with a copper-source Philips automated powder diffractometer. Semi-quantitative mineral abundance was determined using integrated peak areas and empirical reference intensity ratio factors. Gamma-ray and resistivity profiles for the cored intervals were collected by the respective companies when the wells were drilled and were accessed through publicly available records. Depth profiles of aluminum (Al), calcium (Ca), iron (Fe), potassium (K), molybdenum (Mo), silicon (Si), titanium (Ti), zirconium (Zr), and vanadium (V) were assessed at the University of Alberta with a Niton XL3t XRF Analyser. For XRF analysis, outcrop samples were collected at an interval of 0.1 m to 2 m, with higher resolution in intervals of greater interest (e.g., the Hare Indian and Canol Formations). These samples were then pulverized and placed into sample capsules with a polypropylene film base. XRF measurements from the cores were collected every 0.1 m, and the core was washed in the areas of analysis. Outcrop and core samples were then analysed with XRF for 180 seconds in the mining mode. The analyser was purged with helium during analysis to increase the detection of light elements. The United States Geological Survey Brush Creek Shale (SBC-1) was used as a reference material to monitor accuracy and precision. For each element, the measured mean, the error reported as two standard deviations from the mean (2σ), and certified values for SBC-1 are reported in Appendix B. Enrichment factors for a given element (X) are calculated according to Equation 1 (e.g., Brumsack, 2006; Tribovillard et al., 2006). In this study, we calculated enrichment factors for Mo and V and used the Post-Archean Average Australian Shale (PAAS) for the average shale values, which gives an average of 84,000 ppm Al, 1 ppm Mo, and 140 ppm V (Taylor & McLennan, 1985).

$$EFX = (X/Al)_{sample}/(X/Al)_{average\ shale} \quad \text{(Equation 1)}$$

Our XRF dataset for the Hare Indian Formation (the lowermost of the three formations comprising the Horn River Group) was previously published in Harris et al. (2021). In this study, we present for the first time XRF results from the two upper formations in the Horn River Group (the Ramparts and Canol Formations), in addition to XRF results from the overlying Imperial Formation, amounting to more than 5,000 new XRF measurements across nine cores and outcrops. We include the previously published results from the Hare Indian Formation from Harris et al. (2021) to allow for a robust sequence stratigraphic analysis of the entire Horn River Group and comparison of geochemical and sedimentological results. This study follows sequence stratigraphic nomenclature as summarized by Catuneanu (2019).

3.4. Chemostratigraphic proxies

Nine elements were considered as geochemical proxies: Al, Ca, Fe, K, Mo, Si, Ti, Zr, and V. In mudstone units, the elements often associated with the detrital fraction

include Al, Fe, K, Ti, and Zr (e.g., Ratcliffe et al., 2012a; Sano et al., 2013); these elements were selected as potential proxies for terrigenous sediment supply. The ratio of Ti to Al was also included to assess the relative abundance of heavy minerals compared to aluminosilicate minerals, which may vary with aeolian dust input (e.g., Wehausen & Brumsack, 1999) or changes in fluvial discharge (Sageman & Lyons, 2003). Vanadium and Mo are redox-sensitive trace metals that become enriched under reducing conditions; their abundance is commonly used as a proxy for paleoredox conditions (e.g., Algeo & Liu, 2020; Tribovillard et al., 2006). Moreover, Ca was included here as a proxy for carbonate mineral content, and Si was considered as a proxy for quartz and aluminosilicate content. Trends in Si were compared with those of Al to assess the presence of excess (non-aluminosilicate) Si, which can be derived from aeolian, biogenic, or hydrothermal sources (e.g., Adachi et al., 1986; Sageman & Lyons, 2003). In this study, Principal Component Analysis (PCA) was used to assess the covariance between the elemental proxies and to select the most useful proxies for comparison with sequence stratigraphic interpretations. Highly skewed variables were log-transformed, and the "prcomp" function of the R programming language was used to perform PCA of the dataset.

Normalizing certain elements (e.g., Si, Ti, Mo, V) to Al can be useful for comparing their abundance to detrital aluminosilicate abundance. However, normalizing to Al can produce apparent correlations between unrelated elements, especially if the coefficient of variation (CV) for Al is large compared to that of the normalized elements (Van der Weijden, 2002). In our dataset, the CV of Al ranges from 25 % to 66 % depending on the core or outcrop, with an average of 47 % (Appendix B). This is similar to the CV for Ti (28 % to 74 %, average of 47 %) and lower than the CV for Mo (35 % to 174 %, average of 76 %) and V (37 % to 122 %, average of 66 %) and thus, these elements were normalized to Al for presentation in the results figures (Appendix B). Titanium was normalized directly to Al, whereas Mo and V were normalized to Al and an average shale value (Equation 1). In contrast, the CV of Si ranges from 12 % to 54 %, with an average of 28 % (Appendix B), and thus, it was not normalized Al. Instead, we identified intervals of excess Si by comparing the trends in Si and Al.

4. Results

4.1. Sedimentological and mineralogical results

We identified six lithofacies in the Horn River Group and the lowermost Imperial Formation in our study area (Figure 2; Table 1). The lithofacies (LF) are: (LF1) light grey tentaculitoid grainstone intercalated with dark grey calcareous to calcareous siliceous mudstone; (LF2) medium grey planar parallel-laminated calcareous to siliceous calcareous mudstone; (LF3) brownish black continuous planar parallel-laminated siliceous mudstone with common calcareous/dolomitic laminae and cm-scale carbonate beds; (LF4) brownish black continuous planar parallel-laminated siliceous mudstone; (LF5) medium dark grey planar parallel laminated fissile argillaceous to siliceous intraclasT–Rich mudstone; and (LF6) medium grey homogenous-appearing fissile argillaceous to siliceous mudstone with common fossil fragments.

Following the scheme presented in Biddle et al. (2021), the thin sections included in this study were classified as one of the following seven microfacies (MF): (MF1) homogeneous-looking radiolarian-rich fine mudstone; (MF3) discontinuous wavy parallel to homogeneous-looking fine mudstone; (MF4) rarely bioturbated discontinuous wavy parallel silt-bearing fine mudstone; (MF5) bioturbated discontinuous wavy parallel silt-bearing fine mudstone; (MF6) bioturbated discontinuous planar parallel to continuous wavy non-parallel medium mudstone; (MF7) fossiliferous discontinuous to continuous wavy parallel fine mudstone; or (MF8) fossiliferous discontinuous to continuous wavy parallel fine mudstone (Appendix A). In the present study, Microfacies 2 (MF2) from Biddle et al. (2021) has been reclassified as a diagenetic overprinting of other microfacies (Appendix A). Where possible, instances of MF2 have been reassigned to other microfacies.

In the N-09 core, which has high thin section coverage relative to the other cores and outcrops, relationships between lithofacies and microfacies can be readily observed (Figure 3). Certain lithofacies (e.g., LF3, LF4, and LF6) are characterized by more than one microfacies. In other lithofacies, a single microfacies was observed. For example, LF1 strata are primarily characterized by MF7, and LF5 is exclusively characterized by MF8 (Figure 3). Table 1 includes a summary of all lithofacies and microfacies relationships from the N-09 and O-06 cores.

4.2. Multivariate statistical results

PCA results from the Horn River Group (Hare Indian, Canol, and Ramparts Formations) and the lowermost Imperial Formation are displayed in Figure 4. Principal component 1 (PC 1) explains 45.4 % of the variance in the Canol Formation dataset, 48.3 % of the variance in the Hare Indian Formation, 40 % in the Imperial Formation, and 75.2 % in the Ramparts Formation. Principal component 2 (PC 2) accounts for 27.4 %, 22.8 %, 26.8 %, and 9.8 % of the variance in the Canol, Hare Indian, Imperial, and Ramparts Formations datasets, respectively. In all four plots, Al, Fe, K, Ti, and Zr are clustered together (Figure 4). In the Canol, Hare Indian, and Imperial Formations, Mo and V plot near one another, although in the Ramparts Formation, V covaries with Al, K, Ti, and Zr rather than Mo (Figure 4). Silicon is present in a similar zone to V and Mo in the Canol, Hare Indian, and Imperial Formations, but plots near Al, K, Ti, and Zr in the Ramparts Formation.

Name	Mineralogy	Sedimentology and Accessories	Fossils and Bioturbation	Associated Microfacies	Depositional environment (based on microfacies interpretations from Biddle et al., 2021)
LF1: Light grey tentaculitoid grainstone intercalated with dark grey calcareous to calcareous siliceous mudstone	• Quartz: 5 – 31 %, μ = 14 % • Carbonate: 46 – 89 %, μ = 74 % • Total clay: 6 – 23 %, μ = 12 % • n = 3	• Laminae are wavy discontinuous non-parallel or continuous and discontinuous planar parallel • Tentaculitoid beds are sometimes graded, with an upwards decrease in the abundance of tentaculitoids • Soft-sediment deformation structures occasionally observed (ball and pillow structures, load casts occasionally present at base) • Cone-in-cone structures may be present • Non-fissile to low-fissility	• Tentaculitoid beds and laminae • Bioturbation not observed with the naked eye	Primarily MF7 with some occurrences of MF6	Deposition by a combination of low-density turbidites, plug-like flows, and debrites suggestive of a storm-influenced shelf setting.
LF2: Medium grey planar parallel-laminated calcareous to siliceous calcareous mudstone	• Quartz: 19 – 44 %, μ = 31 % • Carbonate: 29 – 76 %, μ = 52 % • Total clay: 5 – 16 %, μ = 16 % • n = 2	• Planar parallel laminae common • Stylolites parallel and co-current with bedding planes • Non-fissile	• Bioturbation not observed with the naked eye	MF5, MF6, and MF7	Deposition from plug-like flows and low-density turbidity currents on the storm-influenced shelf in an adjacent but more distal position relative to LF1.
LF3: Brownish black continuous planar parallel-laminated siliceous mudstone with common calcareous/dolomitic laminae and cm-scale carbonate beds	• Quartz: 8 – 93 %, μ = 74 % • Carbonate: 6 – 58 %, μ = 20 % • Total clay: 6 – 58 %, μ = 20 % • n = 118	• Common calcareous/dolomitic laminae or cm-scale limestone/dolostone beds • Common calcite/dolomite and pyrite nodules (often have both carbonate and pyrite in same nodule) • Stylolites common on bedding planes • Planar parallel laminae common • May also appear homogeneous • Pyrite streaks sometimes present • Low-moderate fissility	• Pyritized tentaculitoids are rarely observed on bedding planes • Bioturbation not observed with the naked eye	Primarily MF3, with some occurrences of MF1, MF4, and MF5	Deposition from storm-wave resuspension of unconsolidated, water-rich muds and pelagic suspension settling in a more distal shelf position relative to LF1 and LF2.
LF4: Brownish black continuous planar parallel-laminated siliceous mudstone	• Quartz: 30 – 91 %, μ = 63 % • Carbonate: 0 – 57 %, μ = 8 % • Total clay: 7 – 51 %, μ = 29 % • n = 33	• Planar parallel laminae common but sometimes also appears homogeneous • Abundant pyrite streaks • Pyrite nodules common • Occasional calcareous or dolomitic laminae • Rare limestone/dolostone nodules • Low-moderate fissility	• Bioturbation not observed with the naked eye	MF4, MF5, and MF6	Deposition from plug-like flows, low-density turbidites, and debrites, suggesting deposition in an intermediate shelf position, more distal than LF2 and LF1, but more proximal than LF3.
LF5: Medium dark grey planar parallel laminated fissile argillaceous to siliceous intraclasT–Rich mudstone	• Quartz: 1 – 67 %, μ = 42 % • Carbonate: 0 – 17 %, μ = 4 % • Total clay: 30 – 99 %, μ = 54 % • n = 14	• Occasional pyrite nodules • Moderate-high fissility • Planar parallel laminae are common • Intraclasts often present along laminae • Rare calcareous laminae	• Rare Spathiocaris fossils on bedding planes • Bioturbation not observed with the naked eye	MF8	Deposition from high energy, intraclast-generating erosive bottom currents in a proximal shelf to distal delta setting.
LF6: Medium grey homogeneous-appearing fissile argillaceous to siliceous mudstone with common fossil fragments	• Quartz: 28 – 71 %, μ = 48 % • Carbonate: 0 – 14 %, μ = 1 % • Total clay: 27 – 72 %, μ = 51 % • n = 27	• Often appears homogeneous, but planar parallel laminae also present • Pyrite nodules common • Occasional dolomitic laminae or cm-scale beds • High fissility	• Fossil fragments (including Spathiocaris) common on bedding planes • Bioturbation not observed with the naked eye	Primarily MF3, with minor occurrences of MF4	Deposition from storm-wave resuspension of unconsolidated, water-rich muds in a similar but more proximal shelf position relative to LF3.

Table 1 | Characteristics of the six lithofacies identified in the Horn River Group and lowermost Imperial Formation in the I-78, N-09, N-20, and O-06 cores. Quartz, total clay, and carbonate are normalized to 100 wt %, with n denoting the sample size and μ representing the mean. This lithofacies scheme is modified from Harris (2020), which includes a summary of lithofacies in the Hare Indian Formation of the Horn River Group, from Biddle et al. (2021), which presented microfacies for the Horn River Group, and from LaGrange et al. (2022), which summarized lithofacies in the N-09 core of the Horn River Group. Acronyms and abbreviations: LF – lithofacies and MF – microfacies.

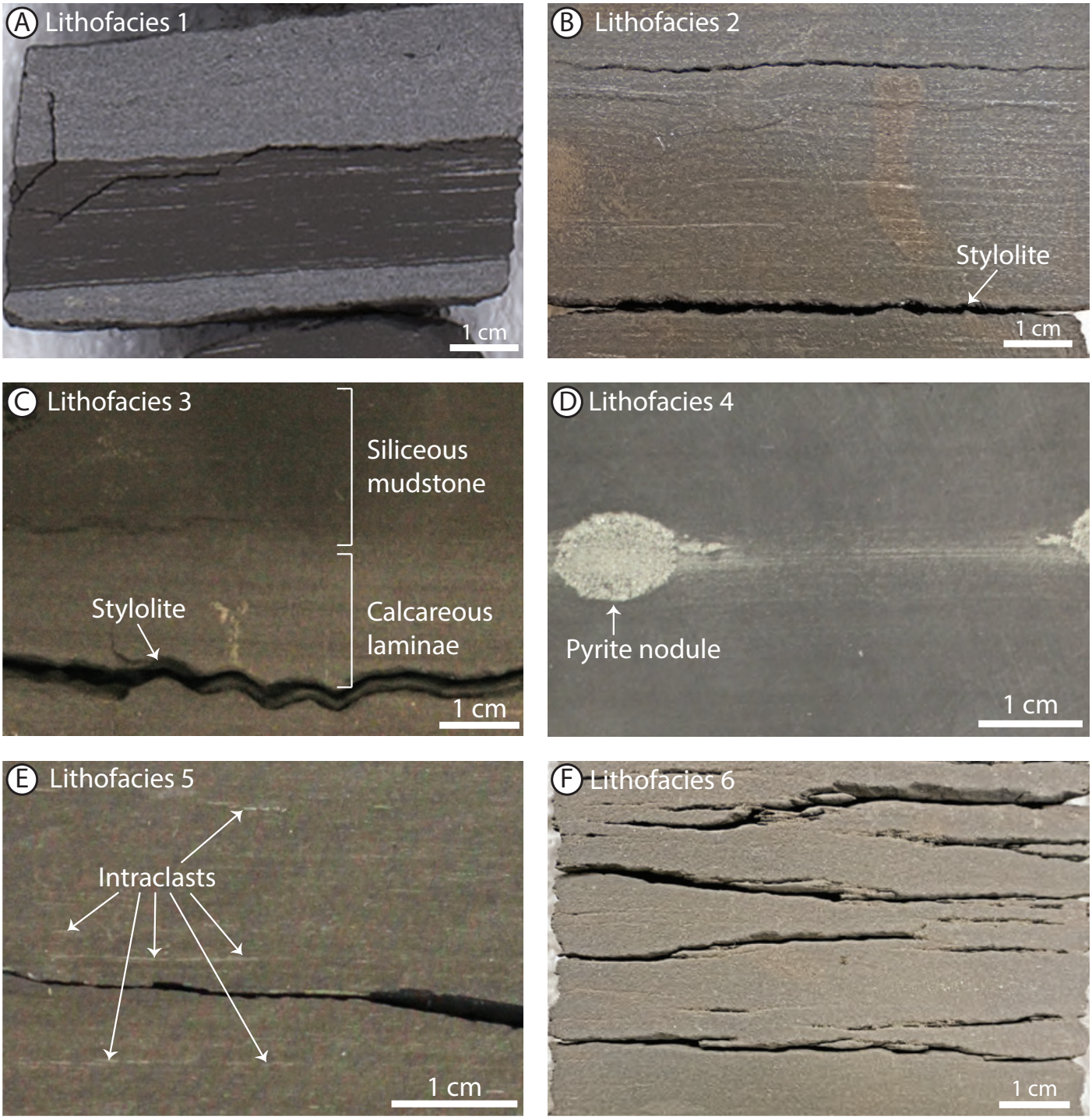

Figure 2 | Representative photographs showing the six lithofacies identified in the Horn River Group and overlying Imperial Formation of our studied cores. (A) Tentaculitoid grainstone intercalated with calcareous to calcareous siliceous mudstone in Lithofacies 1 at a depth of 1823.3 m in the Bluefish Member of the Hare Indian Formation of the N-09 core. (B) A calcareous mudstone of Lithofacies 2 from the N-09 core at a depth of 1777.3 m in the Vermillion Creek Member of the Canol Formation. (C) Lithofacies 3 at 1749.2 m in the Vermillion Creek Member (Canol Formation) of the O-06 core. The image shows a siliceous mudstone with calcareous laminae. (D) A siliceous mudstone characteristic of Lithofacies 4 at 1677.7 m in the Dodo Canyon Member (Canol Formation) of the O-06 core. (E) IntraclasT–Rich laminae in a mudstone sample of Lithofacies 5 from the I-78 core at 1829.2 m in the Dodo Canyon Member of the Canol Formation. (F) A fissile, argillaceous mudstone of Lithofacies 6 at 1696.3 m from the N-09 core in the Imperial Formation.

4.3. Chemostratigraphic results

The profiles of Al, Si, Ca, Ti/Al, EF V, and EF Mo for each core and outcrop are presented in figures 5 to 13, with the full dataset in Appendix B. Of the five detrital proxies considered in PCA (Al, Fe, K, Ti, and Zr), the elements K, Fe, and Zr plot near Al and Ti (Figure 5); therefore, we focus on Al and Ti, as the others exhibit similar trends.

4.3.1. N-09 Core

A series of peaks in Al are present in the N-09 core, and the two most prominent are located in the Francis Creek Member of the Hare Indian Formation and the Imperial Formation (Figure 5). Trends in Si typically show an opposite pattern to Al, and the Ti/Al ratio remains relatively constant. Calcium levels are generally low (< 5 %)

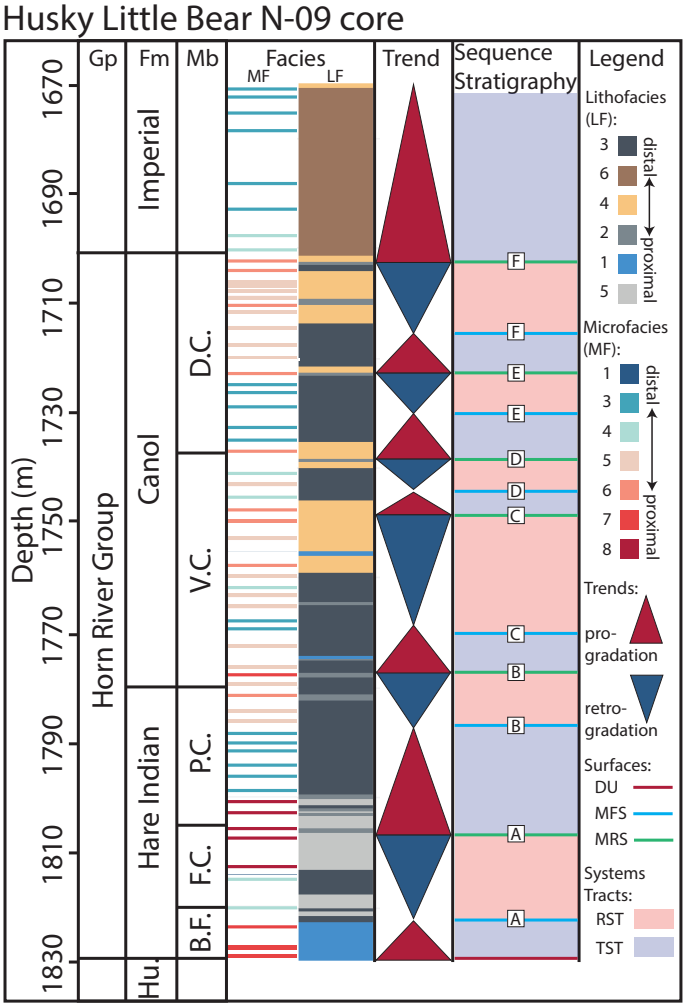

Figure 3 | Microfacies (MF) and lithofacies (LF) results for the Husky Little Bear N-09 core. Interpreted depositional trends are shown to the left, along with interpreted sequence stratigraphic surfaces and systems tracts. Microfacies were interpreted from thin sections by Biddle et al. (2021), with each microfacies line on this figure representing data from one thin section. Acronyms and abbreviations: Gp – group; Fm – Formation, Mb – Member; Hu. – Hume; B.F. – Bluefish; F.C. – Francis Creek; P.C. – Powell Creek; V.C. – Vermillion Creek; D.C. – Dodo Canyon; DU – drowning unconformity; MFS – maximum flooding surface; MRS – maximum regressive surface; RST – regressive systems tract; and TST – transgressive systems tract.

throughout the core, apart from spikes in the Bluefish Member of the Hare Indian Formation and around the Hare Indian–Canol formational contact. Patterns in the enrichment factors for V and Mo generally match one another, with the greatest enrichment in the Dodo Canyon Member of the Canol Formation. However, in the lower half of the Dodo Canyon Member, the peak in EF Mo from 1738 m to 1730 m stratigraphically precedes the EF V peak at 1725 m.

4.3.2. O-06 Core

The Al profile from the O-06 core is characterized by clear fluctuations, with the largest peaks present in the Francis Creek Member (Hare Indian Formation) and Imperial Formation (Figure 6). Silicon shows the reverse trends to Al, with the highest Si at depths where Al is lowest. The Ca profile shows peaks in the lower half of the Hare Indian Formation, at the Hare Indian–Canol formational contact, and again at the contact between the Vermillion Creek Member and Dodo Creek Member in the Canol Formation. Aside from higher Ti/Al values in the Hume Formation carbonates underlying the Horn River Group, the ratio of Ti to Al is steady throughout the Hare Indian, Canol, and Imperial Formations. Together, the EF V and EF Mo redox proxies show several coincident peaks in enrichment, most prominently at 1800 m in the upper Bluefish Member (Hare Indian Formation) and 1691 m in the middle of the Dodo Canyon Member (Canol Formation). Additionally, in both the Powell Creek Member (Hare Indian Formation) and the lower portion of Dodo Canyon Member (Canol Formation), there are peaks in EF Mo a few meters below peaks in EF V.

4.3.3. N-20 Core

Aluminum in the N-20 core follows a similar pattern as in the N-09 and O-06 cores, with a large spike in the Francis Creek Member, lower-magnitude cycles throughout the Powell Creek Member and Canol Formation, and another large peak in the Imperial Formation (Figure 7). Again, the Si profile shows opposite trends relative to Al. In this core, Ca follows a similar pattern as in the O-06 core, with highest values in the lower interval of the Hare Indian Formation, and lower magnitude peaks at the Hare Indian to Canol formational transition, and at the top of the Vermillion Creek Member. The ratio of Ti to Al is generally stable in the Hare Indian, Canol, and Imperial Formations, except for a peak at the base of the Hare Indian Formation at the contact with the underlying Hume Formation. Enrichment factors for V and Mo exhibit similar profiles as in the O-06 core, with several peaks and troughs, most of which align at the same depths. In two intervals (the Powell Creek Member and lower Dodo Canyon Member), the highest EF Mo values occur roughly 10 m below the highest EF V results.

4.3.4. I-78 Core

The I-78 core includes the Bluefish Member at the base of the Hare Indian Formation and the upper portion of the Canol Formation, separated by an unretrieved gap of core spanning approximately 60 m (Figure 8). The Si, Al, and Ca profiles in the Bluefish Member are characterized by repeated fluctuations superimposed upon larger-scale trends. From the base of the core moving upward through the Bluefish Member, Al and Ca generally decrease while Si increases, until a shift at 1955 m marks a reversal: Al and Ca begin to rise, and Si declines. The ratio of Ti/Al has low variability in the Bluefish Member, aside from small peaks around 1947 m and 1938 m. In the Canol Formation, Al and Si covary negatively, and Ti/Al is generally steady. Trends in EF V and EF Mo are aligned in both the Bluefish Member and Canol Formation intervals of the I-78 core.

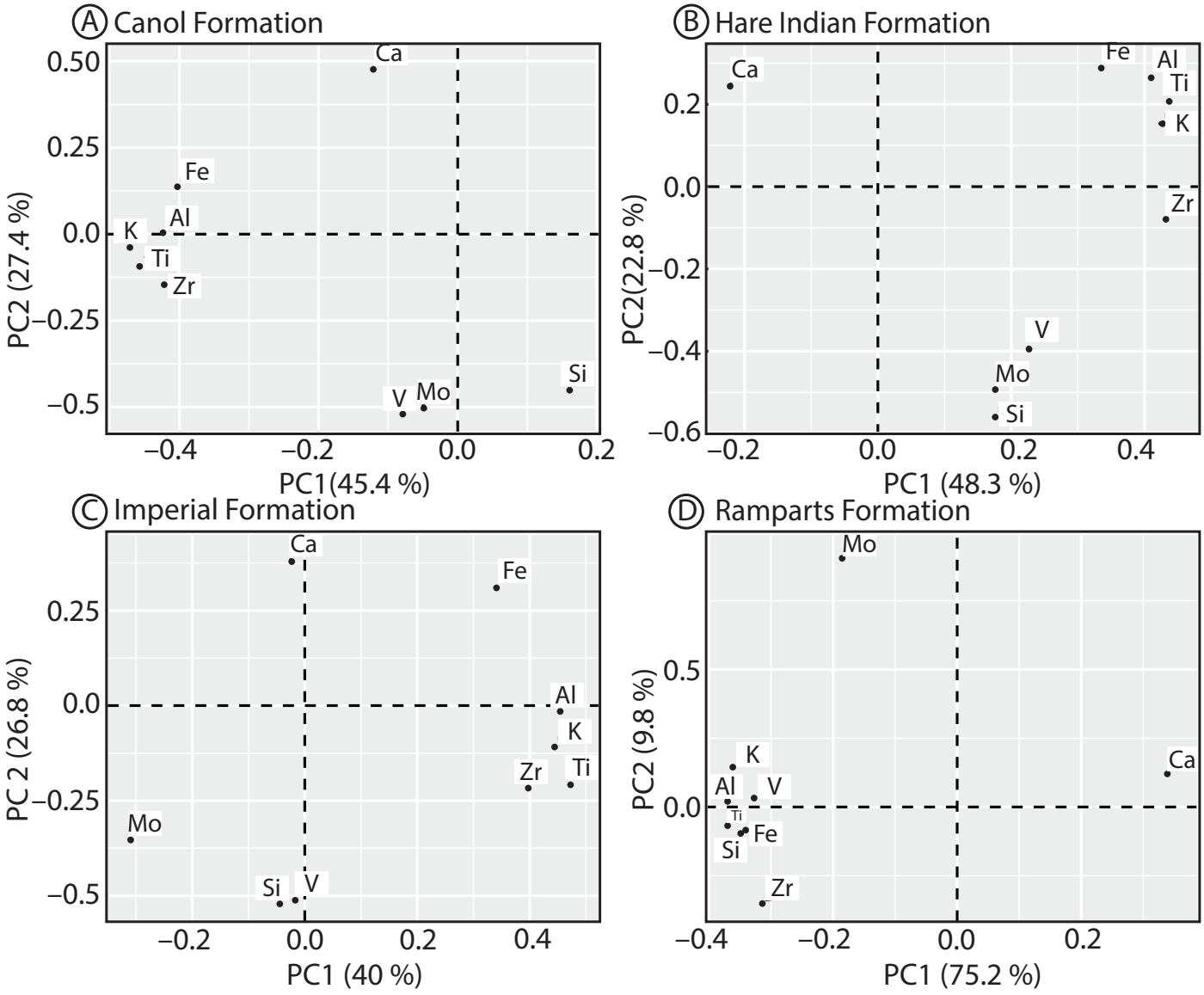

Figure 4 | Principal Component Analysis results show the covariance between elements from (A) the Canol Formation, (B) the Hare Indian Formation, (C) the Imperial Formation, and (D) the Ramparts Formation. Acronyms: PC – principal component.

4.3.5. Carcajou River Outcrop

As with the cores, Al and Si show opposite trends throughout the Canol and Imperial Formations at the Carcajou River outcrop (Figure 9). The Canol Formation is characterized by smaller magnitude cycles in the abundance of Al and Si, whereas the overlying Imperial Formation contains a larger magnitude peak in Al and decrease in Si at approximately 87 m. The Ca profile does not show any remarkable peaks throughout the section and is characterized by a subtle decrease from the lower to the upper Canol Formation. The Ti/Al profile is steady throughout the sampled interval. Enrichment factors for the redox-sensitive trace metals V and Mo show three peaks in the upper half of the Canol Formation. The upper two peaks in EF V and EF Mo occur at the same depths as one another (at ~ 77 m and ~ 65 m), but the lowermost spikes in EF V and EF Mo are offset from each other by approximately 5 m.

4.3.6. Dodo Creek outcrop

In the section sampled at Dodo Creek, Al and Si negatively covary and are characterized by repeated fluctuations in their abundance (Figure 10). Calcium peaks at around 20 m in the lower Canol Formation and shows a clear decrease from the lower to the upper Canol Formation. In contrast, the Ti/Al ratio is steady and shows little variability throughout the Canol Formation and lower Imperial Formation. The enrichment factors for V and Mo show cycles of increase and decrease in the Canol Formation, which mostly align with one another, except in the interval from 67 to 80 m, where the peak in EF Mo precedes the peak in EF V by roughly 10 m.

4.3.7. Mountain River Outcrop

A continuous section of the Horn River Group is present at Mountain River, and is entirely accessible, apart from one short interval at the top of the Hare Indian Formation (Bell Creek Member), which could not be sampled because of its recessive nature and thick vegetation cover.

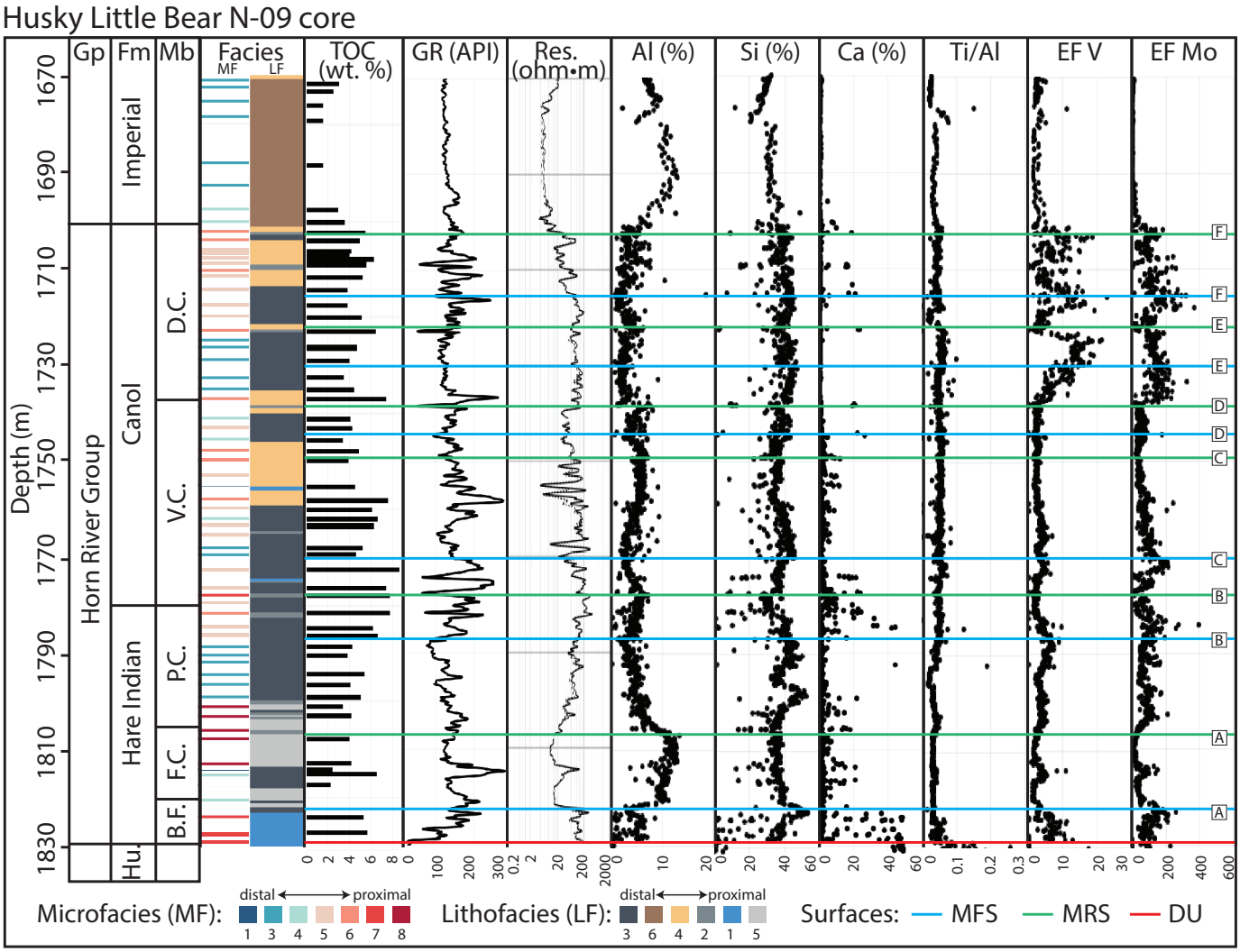

Figure 5 | Microfacies (MF), lithofacies (LF), total organic carbon (TOC), gamma-ray log, resistivity log, and X-ray fluorescence results for the Husky Little Bear N-09 core. Microfacies were interpreted from thin sections by Biddle et al. (2021), with each microfacies line on this figure representing data from one thin section. The solid line on the resistivity plot represents shallow resistivity (10″), whereas the dashed line is associated with deep (90″) resistivity. Acronyms and abbreviations: Gp – group; Fm – Formation, Mb – Member; Hu. – Hume; B.F. – Bluefish; B.C. – Bell Creek; F.C. – Francis Creek; P.C. – Powell Creek; V.C. – Vermillion Creek; D.C. – Dodo Canyon; MF – microfacies; LF – lithofacies; TOC – total organic carbon; GR – gamma ray; Res. – resistivity; EF V – V enrichment factor; EF Mo – Mo enrichment factor; MFS – maximum flooding surface; MRS – maximum regressive surface; and DU – drowning unconformity.

The lowermost Bluefish Member is characterized by low Al, high Si, EF V, and EF Mo, which shifts to increasing Al and decreasing Si, EF V, and EF Mo moving upwards in the Hare Indian Formation (Figure 11). In contrast to the other cores and outcrops, Al does not peak in the middle of the Hare Indian Formation and instead continues to increase upward towards the unsampled interval at the top of the Bell Creek Member. Calcium is variable throughout the Hare Indian Formation, with highest values in the lower Bluefish Member. The Horn River Group at Mountain River also includes the platform carbonates of the Ramparts Formation, which are characterized by variable but generally decreasing Al and Si, combined with low enrichment factors of V and Mo. Calcium also fluctuates in the Ramparts Formation, with an overall increasing upwards trend. Above the Ramparts interval (in the Canol and Imperial Formations), the geochemical proxies exhibit similar trends as in the other cores and outcrops: (1) Si and Al show similar but opposite patterns, with smaller magnitude cycles in the Canol Formation and a larger magnitude peak in Al near the Canol–Imperial contact, (2) Ca shows generally higher values in the lower Canol Formation relative to the upper Canol Formation and Imperial Formation, and (3) highs in EF Mo and EF V occur at several horizons, most of which coincide, except for in the interval from 110 to 120 m. The Ti/Al profile fluctuates very little throughout the interval sampled at the Mountain River outcrop.

4.3.8. Powell Creek outcrop

The Powell Creek outcrop section begins with the Ramparts Formation and was continuously sampled except for an inaccessible gap surrounding the Canol–Imperial formational contact. Like at Mountain River, the Ramparts Formation shows fluctuating, positively covarying Al and Si with an overall upward decrease, and variable Ca with a general upward increase (Figure 12). Relatively little enrichment of V and Mo and steady Ti/Al (i.e., low fluctuation in the ratio and all Ti/Al values below

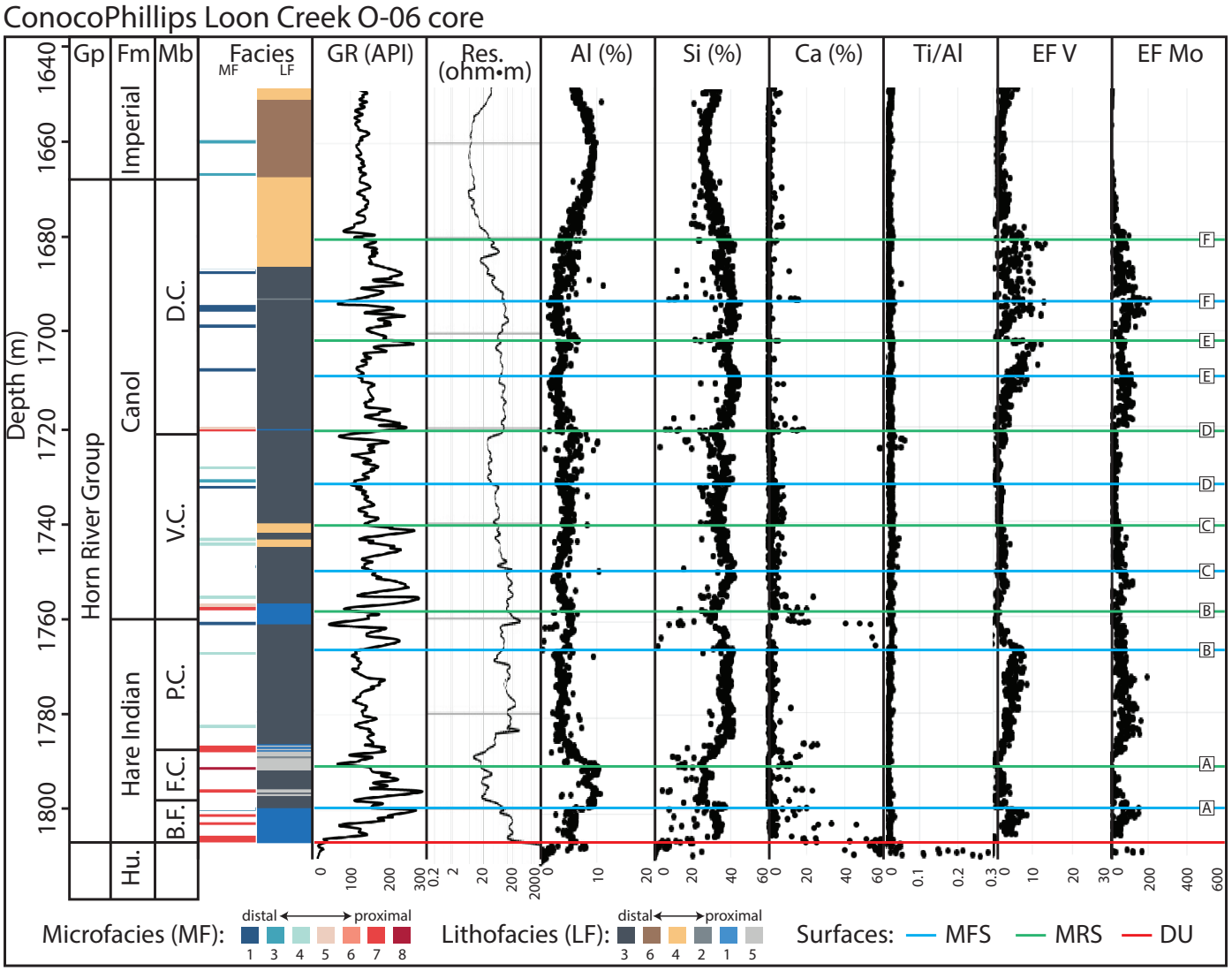

Figure 6 | Lithofacies, gamma ray log, resistivity log, and X-ray fluorescence (XRF) results for the ConocoPhillips Loon Creek O-06 core. The solid line on the resistivity plot represents medium depth resistivity (30″), whereas the dashed line is associated with deep (90″) resistivity. Acronyms and abbreviations: Gp – group; Fm – Formation, Mb – Member; Hu. – Hume; B.F. – Bluefish; B.C. – Bell Creek; F.C. – Francis Creek; P.C. – Powell Creek; V.C. – Vermillion Creek; D.C. – Dodo Canyon; MF – microfacies; LF – lithofacies; TOC – total organic carbon; GR – gamma ray; Res. – resistivity; EF V – V enrichment factor; EF Mo – Mo enrichment factor; MFS – maximum flooding surface; MRS – maximum regressive surface; and DU – drowning unconformity.

0.1) are also observed in the Ramparts Formation at this location. Moving up section, the Canol Formation is initially characterized by relatively low Al and Si concentrations, elevated Ca and Ti/Al values, and generally low enrichment in trace metals. Above ~ 82 m in the Canol Formation, trends in the geochemical proxies return to those observed in the Canol Formation from other cores and outcrops, with increased Si and Al displaying negative covariance, low and steady Ti/Al, and cycles in trace metal enrichments. The Canol–Imperial formational contact was inaccessible at this location, but above 120 m, the Imperial Formation is characterized by increasing Al, decreasing Si, steady Ti/Al, and low enrichment of V and Mo.

4.3.9. Rumbly Creek

Only a short section of the Canol Formation was accessible at Rumbly Creek. This interval is marked by subtle fluctuations in Al, Si, EF V, and EF Mo. As observed in other cores and outcrops, Al and Si show similar but opposite trends to one another. Calcium and the Ti/Al profile are steady throughout the sampled interval, with consistently low values and little fluctuation. Moreover, patterns in the redox proxies are similar to one another, with enrichment in V at similar stratigraphic horizons as peaks in EF Mo.

4.3.10. Chemostratigraphic Summary

The formations comprising the Horn River Group are characterized by distinct chemostratigraphic trends in the cores and outcrops considered in this study. Stratigraphically lowest of the units considered, the Bluefish Member of the Hare Indian Formation typically displays fluctuating Si and Al superimposed upon a larger-scale trend. Overall, there is a Si peak and Al decrease in the Bluefish Member, which corresponds to a horizon of elevated V and Mo enrichment. At locations where the Ramparts Formation is absent, there is a subsequent Al peak and decline in Si toward the middle of the Hare Indian Formation (Francis Creek Member), accompanied

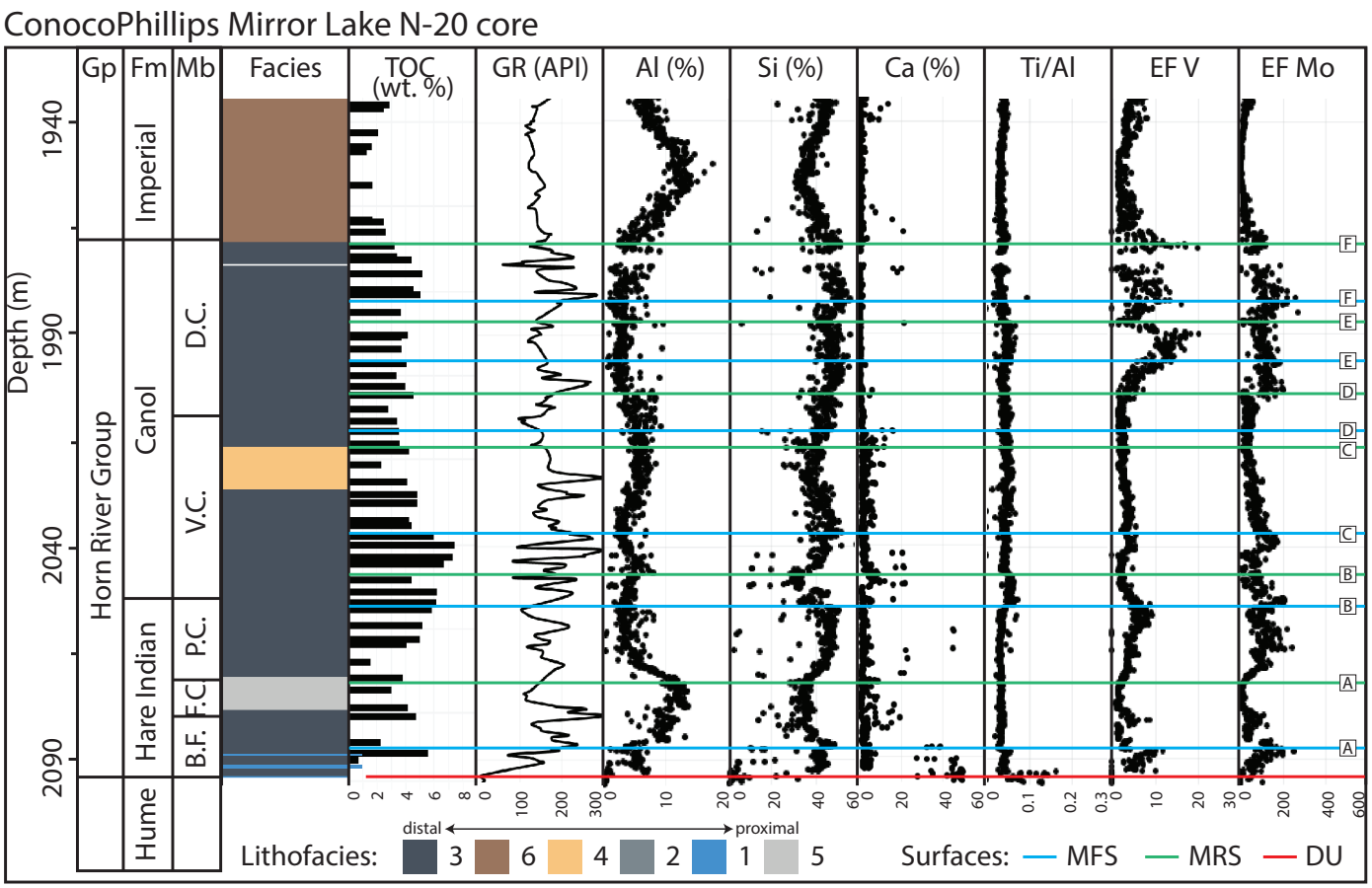

Figure 7 | Lithofacies, total organic carbon (TOC), gamma ray log, and X-ray fluorescence (XRF) results for the ConocoPhillips Mirror Lake N-20 core. Acronyms and abbreviations: Gp – group; Fm – Formation, Mb – Member; B.F. – Bluefish; F.C. – Francis Creek; P.C. – Powell Creek; V.C. – Vermillion Creek; D.C. – Dodo Canyon; TOC – total organic carbon; GR – gamma ray; EF V – V enrichment factor; EF Mo – Mo enrichment factor; MFS – maximum flooding surface; MRS – maximum regressive surface; and DU – drowning unconformity.

by low EF V and EF Mo. Where the Ramparts Formation is present, the peak in Al instead occurs much higher, near the top of the Hare Indian Formation. Calcium in the Hare Indian Formation is always highest in the Bluefish Member, with a few lower magnitude peaks stratigraphically higher up in the formation.

In contrast to the other formations of the Horn River Group, Si and Al show positive covariance in the Ramparts Formation, and this formation is characterized by fluctuating Si and Al concentrations, which generally decrease upward, and very little V or Mo enrichment. Calcium also varies in the Ramparts Formation, with an overall increase in abundance up section.

The Canol Formation displays several cycles in the abundance of Al, Si, EF V, and EF Mo, and the highest enrichment of the redox proxies V and Mo is observed at the top of this interval. In all outcrops and cores, the lower half of the Canol Formation is characterized by higher Ca relative to the upper portion. At Powell Creek, the Ca concentration in the lower half of the Canol Formation is unusually high, with values up to 40%. Additionally, Ti/Al shows very little change in the Horn River Group, aside from a spike in the lower Canol Formation at Powell Creek, which contains limestone turbidites originating from the Kee Scarp Member reefs (Mackenzie, 1970) and sometimes is referred to as the informal 'allochthonous limestone unit'.

Overlying the Horn River Group, the lower Imperial Formation is typically marked by a large peak in Al, coinciding with a decrease in Si. Enrichment of V and Mo declines at the top of the Canol Formation, and the base of the Imperial Formation shows low EF V, EF Mo, and steady Ti/Al. Calcium concentration is mostly low throughout the Imperial Formation, without remarkable trends.

4.4. TOC Results

In the N-09 core, TOC ranges from 1.5 to 8.6 wt. %, with the highest values in the Vermillion Creek Member of the Canol Formation and lowest values in the Imperial Formation (Figure 5; Appendix C). TOC values are slightly lower in the N-20 core than in the N-09 core, ranging from 0.7 to 7.5 wt. %, again with the greatest TOC enrichment in the Vermillion Creek Member and lowest abundance in the Imperial Formation (Figure 7; Appendix C). In the cored intervals of the I-78 well, TOC ranges from 0.4 to 9.2 wt. % and the highest values are associated with the Canol Formation (Figure 8; Appendix C).

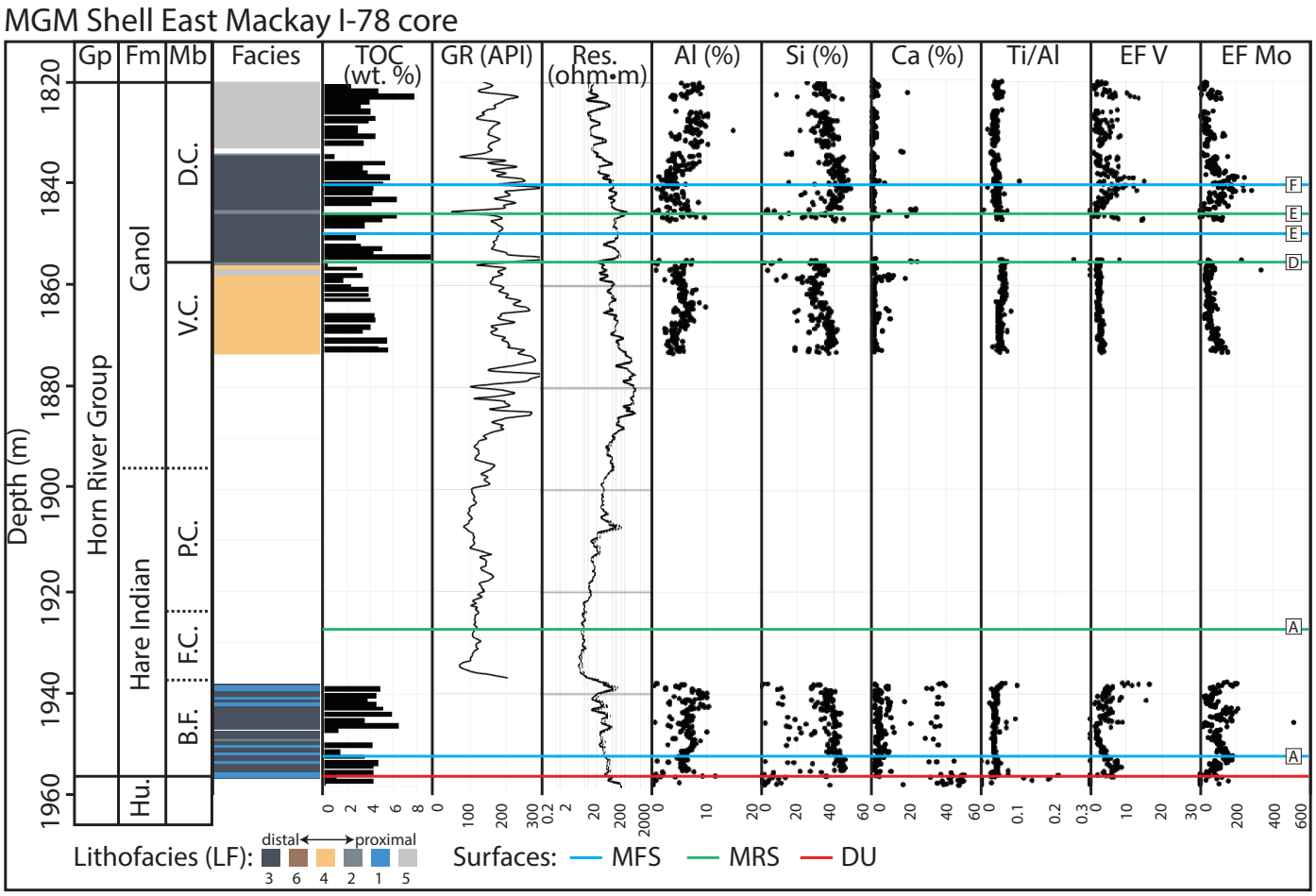

Figure 8 | Lithofacies, total organic carbon (TOC), gamma ray log, resistivity log, and X-ray fluorescence (XRF) geochemical results for the MGM Shell East Mackay I-78 core. The solid line on the resistivity plot represents shallow resistivity (10″), whereas the dashed line is associated with deep (90″) resistivity. Acronyms and abbreviations: Gp – group; Fm – Formation, Mb – Member; Hu. – Hume; B.F. – Bluefish; F.C. – Francis Creek; P.C. – Powell Creek; V.C. – Vermillion Creek; D.C. – Dodo Canyon; TOC – total organic carbon; GR – gamma ray; Res. – resistivity; EF V – V enrichment factor; EF Mo – Mo enrichment factor; MFS – maximum flooding surface; MRS – maximum regressive surface; and DU – drowning unconformity.

4.5. Wireline Results

Gamma log values range from 52 to 284 API in the N-09 core, 7 to 282 API in the O-06 core, and 7 to 301 API in the N-20 core (Figures 5 to 7; Appendix D). The N-09, O-06, and N-20 cores are characterized by the lowest gamma log values at the contact between the Hume Formation and Hare Indian Formation, two peaks in the lower half of the Hare Indian Formation, fluctuating values in the Canol Formation, and relatively steady values around 115 to 130 API in the Imperial Formation. The available gamma profile for the I-78 core extends from the top of the Canol Formation down to the base of the Francis Creek Member in the Hare Indian Formation; no data is available for the base of the Hare Indian Formation or underlying Hume Formation. In the I-78 core, gamma log values range from 50 to 301 API, with lowest values in the upper Hare Indian Formation, and generally higher but fluctuating values in the Canol Formation (Figure 8; Appendix D).

In the N-09 core, shallow resistivity (10″) ranges from 4 to 797 Ω•m, and deep resistivity (90″) spans 4 to 750 Ω•m (Figure 5). Shallow resistivity was not publicly available from the O-06 core. Instead, medium (30″) resistivity values from the O-06 core are between 6 and 1973 Ω•m, whereas the deep (90″) resistivity values range from 6 to 2009 Ω•m (Figure 6). Resistivity results from the N-20 core were not publicly available. The I-78 core is characterized by shallow (10″) resistivity ranging from 4 to 447 Ω•m, and deep resistivity (90″) from 5 to 444 Ω•m (Figure 8). Patterns in resistivity are similar between the N-09, O-06, and N-20 cores, with higher values at the base of the Hare Indian Formation in the Bluefish Member and lower resistivity in the upper Hare Indian Formation, transitioning again to higher values in the Canol Formation. Very little offset is observed between the shallow and deep resistivity in the N-09 and I-78 cores (Figures 5 and 8) or between the medium and deep resistivity in the O-06 core (Figure 6).

5. Discussion

5.1. Depositional trends

Biddle et al. (2021) suggest that the Horn River Group mudstone units represent a continuum along the continental shelf (below fair weather wave base) from the most

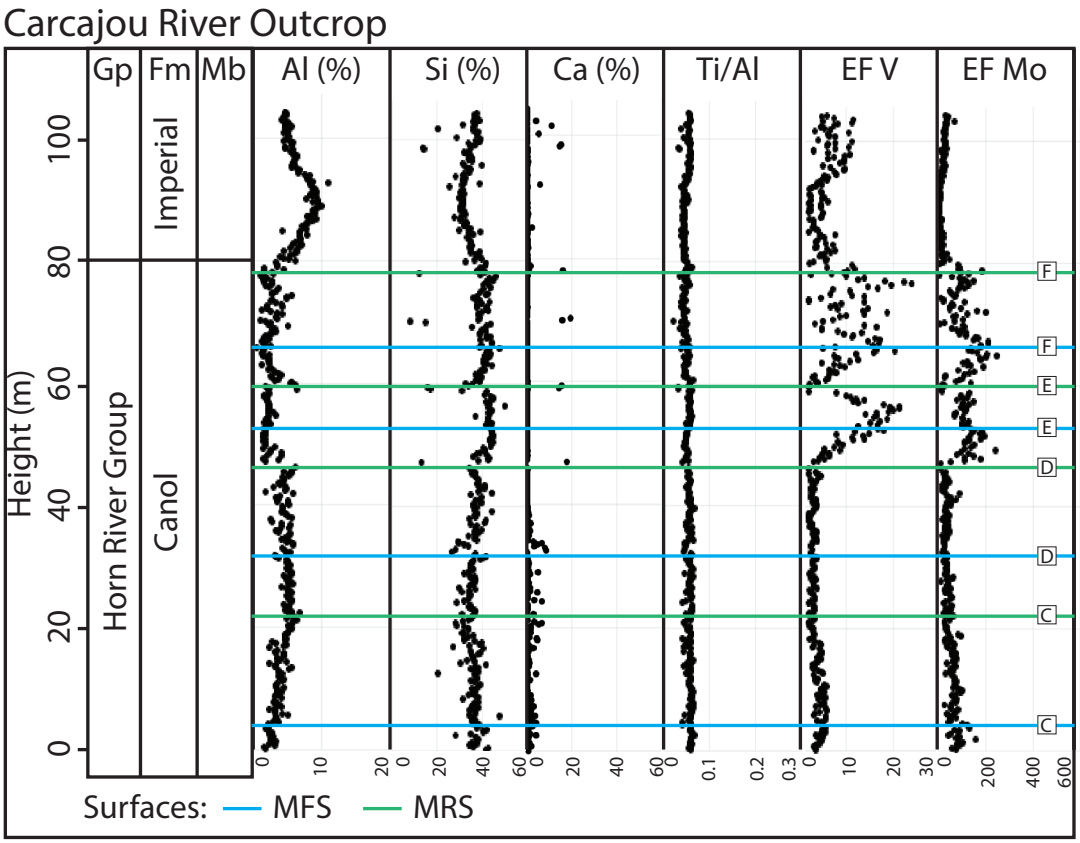

Figure 9 | X-ray fluorescence (XRF) results from the Carcajou River outcrop. Acronyms and abbreviations: Gp – group; Fm – Formation, Mb – Member; EF V – V enrichment factor; EF Mo – Mo enrichment factor; MFS – maximum flooding surface; and MRS – maximum regressive surface.

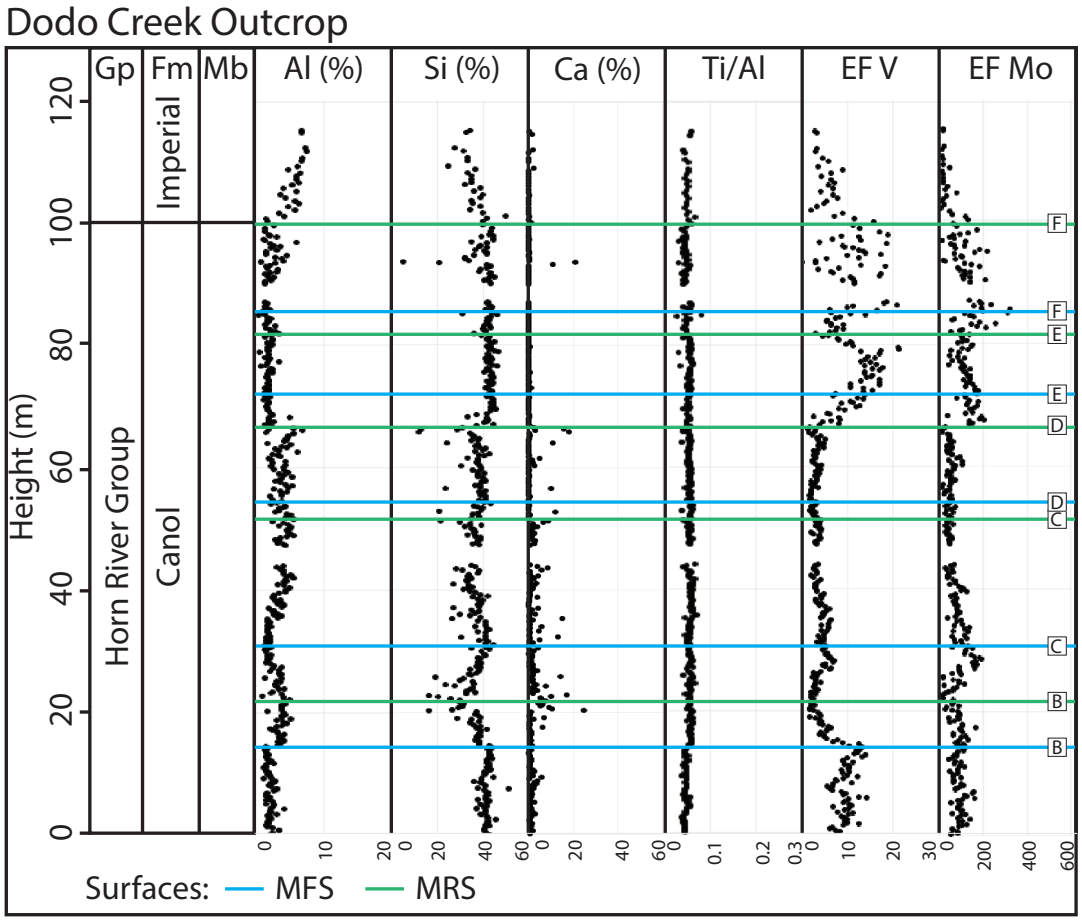

Figure 10 | X-ray fluorescence (XRF) results from the Dodo Creek outcrop. Acronyms and abbreviations: Gp – group; Fm – Formation, Mb – Member; EF V – V enrichment factor; EF Mo – Mo enrichment factor; MFS – maximum flooding surface; and MRS – maximum regressive surface.

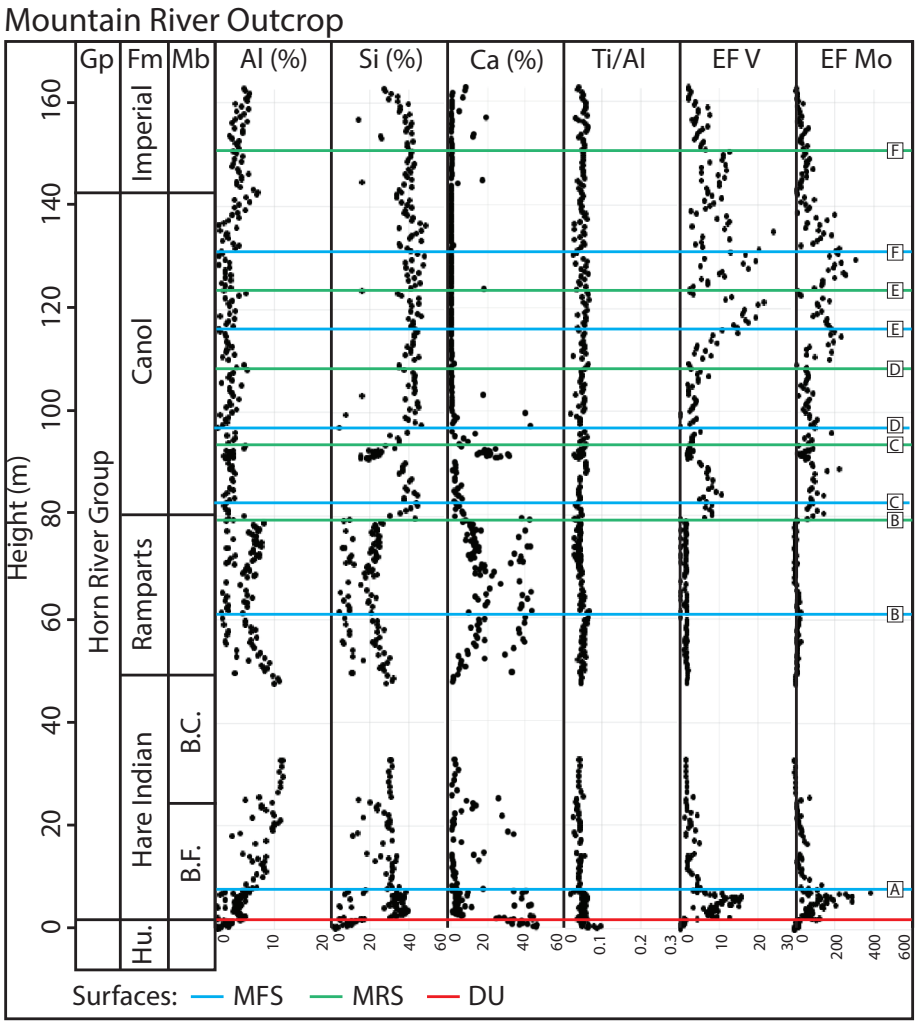

Figure 11 | X-ray fluorescence (XRF) results from the Mountain River outcrop. Acronyms and abbreviations: Gp – group; Fm – Formation, Mb – Member; Hu. – Hume; B.F. – Bluefish; B.C. – Bell Creek; EF V – V enrichment factor; EF Mo – Mo enrichment factor; MFS – maximum flooding surface; MRS – maximum regressive surface, and DU – drowning unconformity.

distal microfacies (MF1), interpreted to be the product of pelagic suspension settling, to intermediate environments with deposition influenced by storm activity (MF2–7), and finally to MF8 deposited in the most proximal environment, possibly associated with the distal reaches of a delta. The present work follows the depositional framework of Biddle et al. (2021), with one notable exception: Microfacies 2 (MF2) was originally interpreted to represent a relatively distal setting with prolonged periods between deposition, leading to the accumulation of early diagenetic dolomite. In this study, we propose the demotion of MF 2 from a formal 'microfacies' to a diagenetic overprinting, which is not considered diagnostic of a particular setting, as it has been observed to overprint several other microfacies (e.g., MF6, MF7, and MF8; Figures 11A, 11B, 11C, 12A, 12B, and 12C in Biddle et al., 2021). Consequently, the interpreted order of microfacies from distal to proximal is MF1, MF3, MF4, MF5, MF6, MF7, and MF8.

Depositional interpretations, which are derived from the microfacies scheme presented in Biddle et al. (2021), are summarized in Table 1. Based on the microfacies observed in each lithofacies, the distal to proximal order of lithofacies on the shelf is interpreted as LF3, LF6, LF4, LF2, LF1, and LF5. In LF6, the occurrence of MF3 and MF4 suggests that the depositional processes and setting resembled those of LF3, in which MF3 is also the most prevalent microfacies. Despite this petrographic likeness, LF6 has significantly higher clay mineral content, with an average of 51 % in LF6 relative to an average of 20 % in LF3 (Table 1). Combined, the microfacies and mineralogy imply that LF6 may have formed in a similar, distal shelf setting relative to LF3, but with a more clay mineral-rich sediment source. Lithofacies 6 is associated with the Imperial Formation and coincides with a transition in tectonic setting from a passive margin to a foreland basin (Beranek et al., 2010; Garzione et al., 1997), supporting the idea that a shift in provenance explains the difference in clay abundance between LF3 and LF6. However, the presence of MF1 (homogenous-looking radiolarian-rich fine mudstone) in LF3 leads to the conclusion that LF3 may have formed in a slightly seaward position compared to LF6. As with LF3, LF4 includes occurrences of MF4 and MF5, but is also composed of MF6, suggesting deposition in an intermediate shelf position relative to the more proximal LF2 and LF1 or the more distal LF3 and LF6. Both LF1 and LF2 are characterized by MF6 and MF7, although LF2 also includes occurrences of the more seaward MF5. Taken together, the prevalence of the more proximal MF7 in LF1 and instances of the more distal MF5 in LF2 suggest that

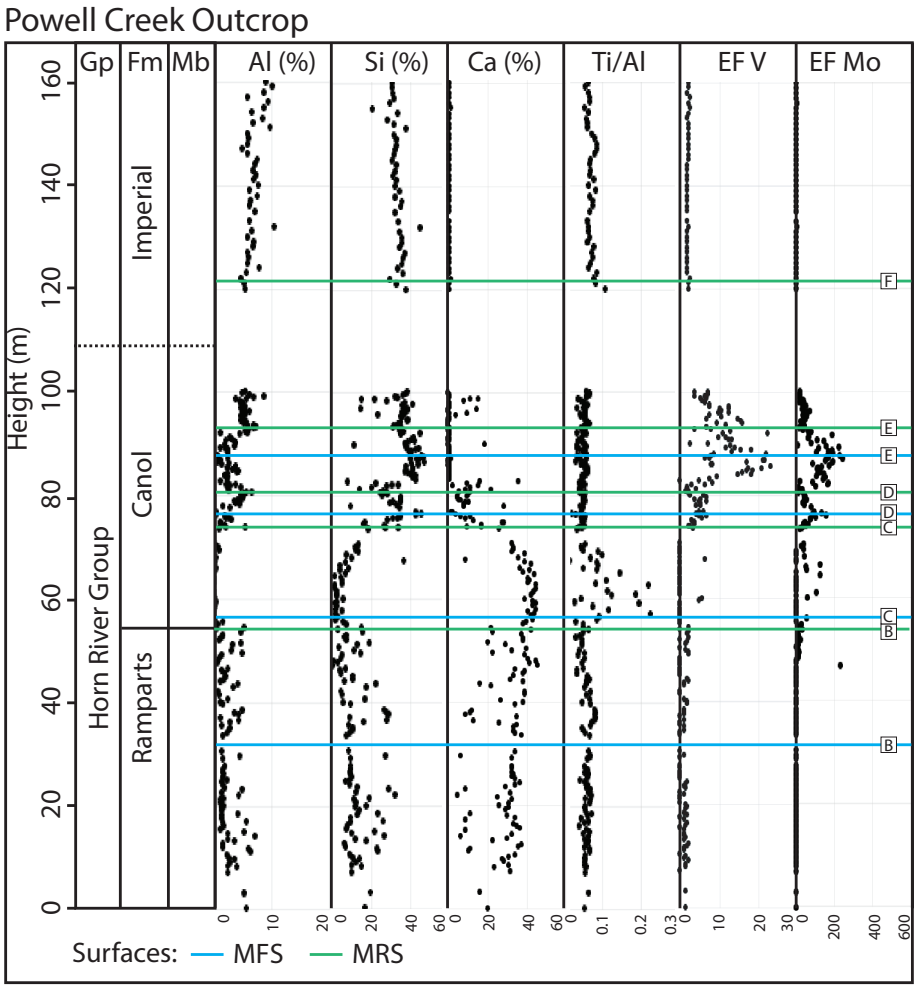

Figure 12 | X-ray fluorescence (XRF) results from the Powell Creek outcrop. Acronyms and abbreviations: Gp – group; Fm – Formation, Mb – Member; EF V – V enrichment factor; EF Mo – Mo enrichment factor; MFS – maximum flooding surface; and MRS – maximum regressive surface.

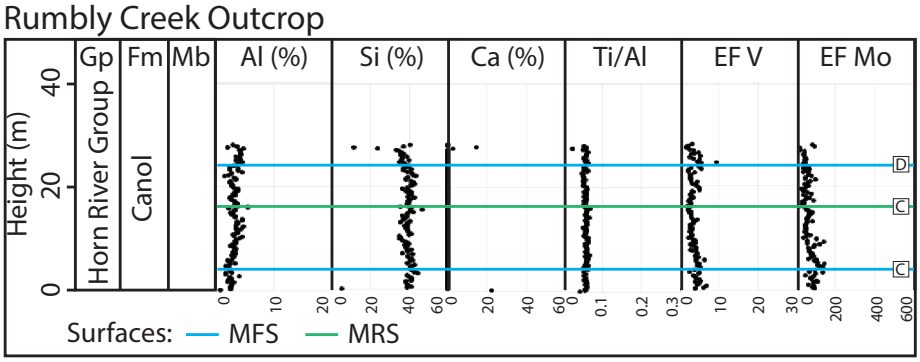

Figure 13 | X-ray fluorescence (XRF) results from the Rumbly Creek outcrop. Acronyms and abbreviations: Gp – group; Fm – Formation, Mb – Member; EF V – V enrichment factor; EF Mo – Mo enrichment factor; MFS – maximum flooding surface; and MRS – maximum regressive surface.

LF1 was deposited in a landward position relative to LF2. Lithofacies 5 is exclusively composed of the most proximal microfacies (MF8) and is thus interpreted as the lithofacies reflecting deposition in the most landward position.

5.2. Sequence stratigraphic interpretation of the N-09 Well

In the N-09 core, high-resolution thin section coverage allows for the identification of depositional trends from shifts in microfacies and lithofacies (Figure 3). Seven progradational trends are indicated by shifts from distal to proximal facies, while six retrogradational trends are marked by facies transitions from proximal to distal (Figure 3). Given that mudstone strata of the Horn River Group represent deposition along the continental shelf, retrogradational trends in shelfal facies are suggestive of transgression at the shoreline; conversely, progradational trends are interpreted as shoreline regression. Six maximum flooding surfaces, marking the switch from transgression to regression (Posamentier & Allen, 1999), are thus identified in strata of the N-09 core and labelled A to F on Figure 3. Maximum regressive surfaces, which separate underlying regressive strata from overlying transgressive deposits

(Helland-Hansen & Martinsen, 1996), are also identified in the N-09 core and labelled A to F (Figure 3). Following previous authors (e.g., Kabanov, 2019; Morrow, 2018; Muir & Dixon, 1984), the transition from the Hume Formation into the Hare Indian Formation is interpreted as a drowning unconformity produced by relative sea-level rise and/or the spread of anoxic waters across the Hume carbonate platform.

Strata above maximum regressive surfaces and below maximum flooding surfaces comprise the transgressive systems tract (TST). In turn, intervals underlain by the maximum flooding surface and overlain by the maximum regressive surface constitute strata of the regressive systems tract (RST; sensu Embry and Johannessen, 1992). Together, these systems tracts represent six complete transgressive–regressive (T–R) sequences in the Horn River Group, with two T–R sequences in the Hare Indian Formation and four T–R sequences in the overlying Canol Formation (Figure 3).

Distinguishing normal regression from forced regression to separate the RST into the highstand systems tract (HST), falling stage systems tract (FSST), and lowstand systems tract (LST) proves challenging with the available dataset. In marine settings, the correlative conformity represents the transition from forced regression to normal regression, and in some instances, can be recognized sedimentologically by a decrease in grain size reflecting a reduction in the volume and size of fluvial sediment reaching the shoreline (Catuneanu, 2022). Regressive strata of the N-09 mudstone core are not characterized by any marked reductions in grain size, suggesting that correlative conformities are not present in the study interval, or are too subtle for recognition. Moreover, the absence of any clear erosive surfaces in the N-09 core suggests that regressive surfaces of marine erosion—the product of wave erosion during forced regression (Plint & Nummedal, 2000)—did not form at the location of the N-09 core during accumulation of the Horn River Group. This may be because wave erosion occurred in a more proximal position relative to the Horn River Group depositional setting, or alternatively, owing to continuous relative sea level rise, an absence of forced regression altogether. Results from the platform and reef units of the Ramparts Formation (which are absent in the N-09 core) support the latter possibility. No evidence of subaerial exposure was observed in the platform and reef carbonates of the Ramparts Formation exposed in the Mackenzie Mountains (Muir, 1988) and Yose et al. (2001) interpreted a series of alternating TSTs and HSTs in the subsurface Ramparts Formation of the Central Mackenzie Valley. Based on conodont biostratigraphy, the upper Hare Indian Formation and lower Canol Formation are time-equivalent to the Ramparts Formation (Kabanov & Gouwy, 2017, 2020), suggesting that at least in these portions of the Hare Indian and Canol Formations, the RSTs are likely HSTs, meaning that relative sea level did not fall and cycles were instead controlled by fluctuations in sediment supply and the rate of relative sea-level rise. These interpretations are consistent with a review by Kabanov et al. (2023), which casts doubt upon the existence of high-frequency eustatic sea-level fluctuations (amplitudes greater than 25 m) during the Middle to Late Devonian.

5.3. Interpretation of chemostratigraphic proxies

In the cores considered here, Al abundance is greatest in lithofacies 6 and 7, which have the highest average clay mineral abundance of the seven lithofacies (Figures 5 to 8; Table 1), lending support to the interpretation of Al as a proxy for terrigenous sediment supply. Overall, the lack of variability in the Ti to Al ratio throughout the Horn River Group and overlying Imperial Formation suggests that the abundance of Ti-hosting phases varies alongside the abundance of aluminosilicates, without instances of significantly increased or decreased heavy mineral supply or preservation compared to aluminosilicates. The only two units characterized by notable increases in Ti/Al are both limestone intervals (the Hume Formation below the Horn River Group and allochthonous carbonate beds in the Canol Formation at Powell Creek), meaning that Ti/Al is also an indicator of shifts between siliciclastic- and carbonate-dominated sedimentation.

The Hare Indian, Canol, and Imperial Formations contain highs in Si that correspond to lows in Al, interpreted to contain 'excess silica' from: (1) aeolian, (2) hydrothermal, or (3) biogenic sources (e.g., Adachi et al., 1986; Sageman & Lyons, 2003). Firstly, marine sediments that contain a higher windblown fraction can be characterized by elevated ratios of Si/Al, Ti/Al, and Zr/Al because quartz, rutile, and zircon are more resistant to physical weathering than clay minerals (Brumsack, 2006; Wehausen & Brumsack, 1999). The excess Si peaks in the Horn River Group and Imperial Formation are not accompanied by peaks in Ti/Al, and as such, we dismiss the possibility that this excess Si is derived from aeolian input. Secondly, excess silica may be hydrothermal in origin. Adachi et al. (1986) demonstrated that hydrothermal cherts could be distinguished from non-hydrothermal cherts and siliceous sediment through an Fe–Al–Mn ternary diagram. When all samples from the Hare Indian, Canol, and Imperial Formations are plotted onto this ternary diagram (Figure 14), most data falls in zone I (non-hydrothermal), with only a few data points falling into the zone II (hydrothermal), likely because these outlier samples contain a high proportion of sulfide minerals (e.g., pyrite nodules). The excess silica in the Hare Indian, Canol, and Imperial Formations is thus best explained by the third possibility: presence of biogenic silica, which in this case is likely derived from the radiolarian tests commonly observed in the Horn River Group (e.g., Biddle et al., 2021; Kabanov, 2019). In the Ramparts Formation, trends in Si typically match those of Al (Figure 4, 11, and 12) and therefore the Si profile is interpreted the same way as the Al profile, as a proxy for terrigenous sediment.

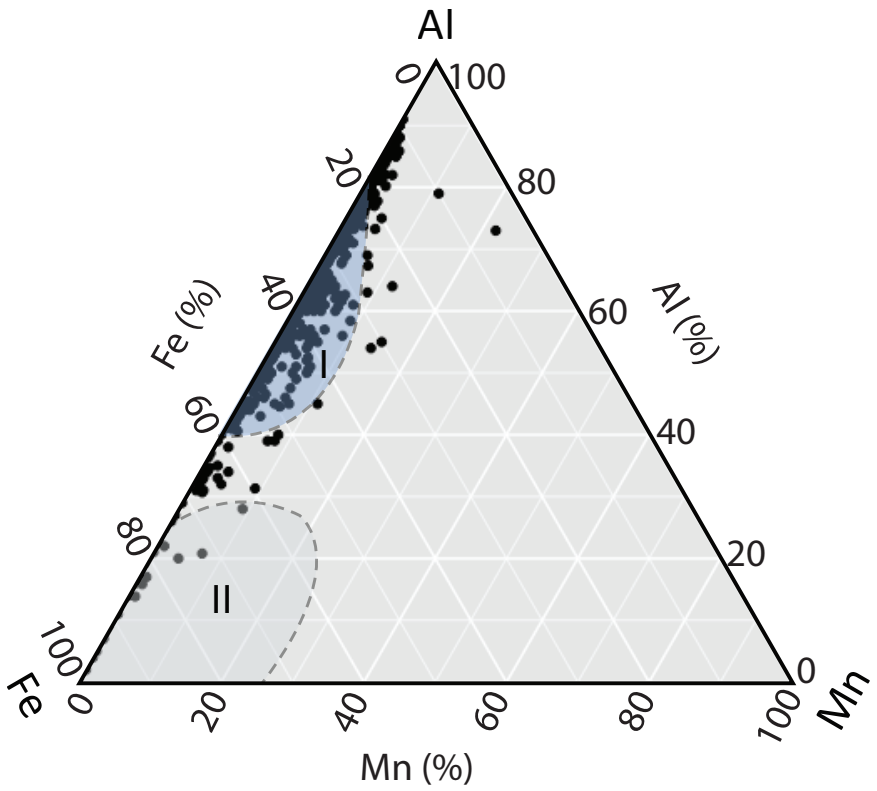

Figure 14 | Fe–Al–Mn ternary diagram for all core and outcrop samples from the Hare Indian, Canol, and Imperial Formations. Field I represents non-hydrothermal cherts and siliceous rocks, whereas field II represents hydrothermal cherts and siliceous rocks. Modified from Adachi et al. (1986) and Arsairai et al. (2016).

In sedimentary successions, patterns in EF V and EF Mo may reflect fluctuations in paleoredox or sedimentation rates. Firstly, V and Mo become more authigenically enriched in seafloor sediment under increasingly reducing conditions (e.g., Scott et al., 2017; Scott & Lyons, 2012). Secondly, through an analysis of fine-grained strata from western Canada and Argentina, Crombez et al. (2020) found that sedimentation rates also influence the accumulation of redox-sensitive trace metals and argued that low sedimentation can cause elevated authigenic trace metal enrichment, which may be unrelated to changes in paleoredox conditions. In the present study, the relationship between microfacies distribution and trace metal enrichment suggests that sedimentation rates were not the primary control on trace metal enrichment (Figure 5). For example, the highest EF V and EF Mo values in the N-09 core are present in the Dodo Canyon Member of Canol Formation (D.C. on Figure 5). In the Dodo Canyon interval, high trace metal enrichment is associated with the most distal microfacies observed in the N-09 core (Microfacies 3). However, similar levels of enrichment are observed in the more proximal Microfacies 5 and 6 (Figure 5), which represent deposition in a position closer to the shoreline, characterized by higher sedimentation rates relative to Microfacies 3 (Biddle et al., 2021). Taken together, the observed patterns of Mo and V enrichment across different microfacies suggest that paleoredox conditions were likely the primary driver of authigenic Mo and V enrichments in Horn River Group strata.

The cores and outcrops included herein are generally characterized by EF V and EF Mo profiles that fluctuate in tandem, except for a few instances where a peak in EF Mo occurs several meters below a spike in EF V. Commonly, an offset between the EF V and EF Mo peaks is present in the mid-Hare Indian Formation and mid-Canol Formation (e.g., in the Powell Creek Member and lower Dodo Canyon Member of the O-06 core shown in Figure 6). These occasional discrepancies between EF Mo and EF V may be explained by the different processes by which the two elements are authigenically enriched in sediment. Vanadium is sequestered in anoxic sediments through the reduction of V(V) to V(IV) and formation of insoluble $VO(OH)_2$, whereas under euxinic conditions, further reduction to V(III) leads to precipitation of V_2O_3 or $V(OH)_3$ (Calvert & Pedersen, 1993; Wanty & Goldhaber, 1992). In contrast, under euxinic conditions, Mo—present in seawater as molybdate (MoO_4^{2-})—reacts with H_2S to form particle-reactive thiomolybdates (e.g., MoS_4^{2-}), which accumulate in sediments through complexation with organic matter or reduced compounds (Erickson & Helz, 2000; Helz et al., 1996). Thus, horizons characterized by peaks in EF Mo preceding peaks in EF V may represent times when anoxia persisted after euxinic conditions subsided, leading to a decline in Mo enrichment but continued sequestration of V into seafloor sediments.

5.4. Chemostratigraphic signatures of sequence stratigraphic surfaces and systems tracts in the N-09 core

In the N-09 core, maximum flooding surfaces are characterized by minima in Al, reflecting low terrigenous sediment input, and maxima in biogenic silica suggested by high Si relative to Al (Figure 5). In contrast, maximum

regressive surfaces A to E show peaks in Al, indicating that these surfaces formed at times of highest terrigenous sediment supply, and low Si compared to Al, suggesting a decreased proportion of biogenic silica at these horizons (Figure 5). However, maximum regressive surface F, present at the transition from the Canol Formation to the Imperial Formation, is instead characterized by low Al and high Si relative to the overlying strata, and coincides with the transition to lithofacies 6 (Figure 5). The Canol Formation to Imperial Formation transition marks the shift in tectonic setting from a passive margin to a retroarc foreland basin (Beranek et al., 2010; Garzione et al., 1997), meaning that maximum regressive surface F is a first-order sequence boundary. The marked increase in Al above maximum regressive surface F and high clay content in lithofacies 6 are indicative of increased terrigenous sediment supply (Figure 5), but the retrogradational trend suggests that this heightened sedimentation rate was outpaced by increased accommodation. Although the Imperial Formation is generally considered to be a progradational unit (e.g., Hadlari et al., 2009), our results suggest that the lowermost portion of this formation (the interval included herein) reflects transgression. This is consistent with the typical early stage of foreland basin evolution, where accommodation produced by orogenic loading and subduction drag forces outpaces sediment supply from the initially low-lying orogeny (Catuneanu, 2004 and references therein).

Regressive systems tracts (above maximum flooding surfaces and below maximum regressive surfaces) are characterized by an upwards-increasing Al profile contrasted by upwards-decreasing Si abundance, suggestive of increasing terrigenous supply and a declining proportion of biogenic silica (Figure 5). Regressive systems tracts (above maximum flooding surfaces and below maximum regressive surfaces) are characterized by an upwards-increasing Al profile contrasted by upwards-decreasing Si abundance, suggestive of increasing terrigenous supply and a declining proportion of biogenic silica (Figure 5).

The calcium profile shows a notable decrease in concentration at maximum flooding surface A and a spike around maximum regressive surface B (Figure 5). No clear shifts in Ti/Al are associated with the interpreted sequence stratigraphic framework, beyond a marked decline in Ti/Al at the basal drowning unconformity associated with the Hume to Hare Indian formational contact (Figure 5). Gamma and resistivity logs show variable signatures at maximum flooding and maximum regressive surfaces.

In contrast, there are noticeable patterns in the enrichment factors for V and Mo relative to sequence stratigraphic surfaces (Figure 5). Maximum flooding surfaces are most often present at or very near peaks in EF V and EF Mo. Above the maximum flooding surfaces, EF V and EF Mo in RSTs typically display either a decreasing pattern or a peak followed by a decrease. Maximum regressive surfaces often occur just below an increase in EF V and EF Mo, with the TSTs above them characterized by increasing EF V and EF Mo moving upwards. The trends observed in EF Mo and EF V imply that the sediment and/or bottom water conditions were mostly reducing, possibly leading to euxinia, during or shortly after the maximum flooding surfaces. As the RST progressed, these conditions became progressively less reducing, followed by a shift towards more reducing conditions after the maximum regressive surface in the TST. An analysis of chemostratigraphic results from previous mudstone studies suggests that the observed pattern in redox conditions is characteristic of an oceanographically open rather than restricted depositional setting (LaGrange et al., 2020), lending further support to the interpretation that the Middle to Late Devonian system of the study area was deposited in an unrestricted marine setting (e.g., Kabanov, 2019; Morrow, 2018). These observations also suggest that in the depositional settings of the Hare Indian, Canol, and lower Imperial Formations, paleoredox conditions varied alongside changes in the balance between relative sea-level rise and sediment supply.

5.5. Sequence stratigraphic correlation

Obtaining high-resolution thin section coverage across several wells and outcrops is rarely feasible, and geochemical signatures are increasingly employed in sequence stratigraphic analyses of mudstone intervals to supplement sedimentological datasets (e.g., B. S. Harris et al., 2021; Li et al., 2021; Milad et al., 2020; Sano et al., 2013; Thöle et al., 2020; Turner et al., 2016; Wang et al., 2022). Aside from the N-09 core, the cores and outcrops considered in this study have limited to no thin section coverage for reasons including budgetary constraints, difficulties in obtaining suitable samples from outcrops characterized by high fissility, and, in certain instances, incorrect preparation of mudstone thin sections. Results from the N-09 core identify the chemostratigraphic signature of sequence stratigraphic surfaces in the Horn River Group, which allows for the interpretation of these surfaces in the other cores from the Central Mackenzie Valley (Figures 5 to 8) and outcrops of the Mackenzie Mountains (Figures 9 to 13). Of the chemostratigraphic proxies considered in the N-09 core, the Al and Si profiles display the most consistent signatures at maximum flooding and maximum regressive surfaces. Trends in those two elements, reflecting the proportion of terrigenous sediment and biogenic silica, are thus used as the primary tools for the sequence stratigraphic interpretation of the other cores and outcrops.

The dataset from the O-06 well provides an opportunity to test the chemostratigraphic signatures derived from the N-09 core. Thin sections from the O-06 core are sparse and preclude a high-resolution sequence stratigraphic interpretation based solely on shifts in microfacies and lithofacies. Guided instead by the chemostratigraphic signatures in the N-09 core, maximum regressive and maximum flooding surfaces were identified in the O-06 core

(Figure 6). At depths where thin sections are present in the O-06, these interpretations agree with the depositional trends indicated by the microfacies distributions, suggesting that in the Horn River Group, Al and Si profiles are reliable indicators of transgressive and regressive trends.

Only two of the nine locations considered in this study—the Mountain River and Powell Creek outcrops—include the carbonates of the Ramparts Formation (Figure 11 and 12). Present between the Hare Indian and Canol Formations, the Ramparts interval is not characterized by the same trends in redox proxies as those observed in the other formations of the Horn River Group or the Imperial Formation. At both outcrops, the Ramparts Formation displays very little enrichment of V and Mo, without clear changes in EF V or EF Mo alongside surfaces or systems tracts (Figures 11 and 12). The lack of enrichment or trends in V and Mo may be explained by less reducing depositional conditions relative to the other formations, possibly from shallower water depths and/or oxygenated water entrained with material shed from the Kee Scarp Member reefs.

Figure 15 shows the correlation between outcrops and cores (A to A' in Figure 1), moving approximately from northwest to southeast. Regressive systems tracts and transgressive systems tracts are interpreted following the criteria identified in the N-09 core, representing six complete T–R sequences between the base of the Hare Indian Formation and the lowermost Imperial Formation (Figure 15). The T–R sequences range in thickness from approximately 10 m to 60 m, with lateral thickness variations (Figure 15). In most T–R cycles (with the exception of T–R cycle 2), the regressive portion of the T–R cycle (RST) is thicker than the transgressive portion (TST). Thickness variations within the same systems tract are attributed to differences in depositional system. RST 1 is thickest at Mountain River outcrop, suggesting higher rates of sediment accumulation compared to the other sections, which is expected given that at this location, RST 1 comprises the Bell Creek Member (distal deltaic mud banks), which is absent in the westward studied cores and outcrops (e.g., Kabanov & Deblonde, 2019; Pyle & Gal, 2016), probably because of increased distance to the clastic sediment source. TST and RST 2 are also thickest at Powell Creek, where there is a thick succession of the Ramparts Formation carbonate strata, which likely experienced higher rates of sediment accumulation compared to the off-bank areas where the other sections were deposited.

The lowermost portion of our sequence stratigraphic interpretation aligns with the previous framework for the Hare Indian Formation by Harris et al. (2021), with one complete T–R sequence identified in the basal Hare Indian Formation. Morrow (2018) interpreted Devonian T–R cycles on a basin-wide scale for the Northern Canadian Mainland Sedimentary Basin (north of 60 ° and westward of the Canadian shield). T–R Cycle B of Morrow (2018) extends from the base of the Hume Formation to the top of the Hare Indian Formation, whereas T–R Cycle C extends from the top of the Hare Indian Formation into the Imperial Formation, with a maximum flooding surface in the Canol Formation (Morrow, 2018). For our study area, the results presented herein suggest that within T–R Cycle C of Morrow (2018), the large-scale maximum flooding surface, and thus the shift from retrogradation to progradation, lies within the Imperial Formation rather than the Canol Formation; i.e., above the units considered in the present study. Moreover, this dataset shows that in the Horn River Group, higher-frequency T–R sequences are superimposed upon the larger-scale basin-wide T–R sequences of Morrow (2018).

In this case study of the Horn River Group, gamma-ray logs do not consistently align with patterns in the detrital clay proxy Al, nor do they routinely correspond with trends in organic matter content or depositional environments (e.g., Figures 5 to 8). Integrating additional datasets (e.g., TOC and detrital proxies) allows the influence of organic matter versus clay minerals to be disentangled, which is otherwise difficult to distinguish in the gamma-ray log profile. In the wells considered herein, resistivity trends sometimes exhibit large-scale inverse relationships with Al concentrations (e.g., in the Francis Creek Member of the Hare Indian Formation and the Imperial Formation). However, there is no clear relationship between patterns in resistivity and trends in facies or geochemical proxies, particularly in the upper Hare Indian and Canol Formations (e.g., Figures 5, 6, and 8). This discrepancy is likely attributed to the range of factors controlling resistivity log readings, including pore fluid properties. While gamma-ray and resistivity logs effectively show broad lithological changes in our study interval—such as transitions from the limestone Hume Formation to the organic-rich, primarily siliciclastic Horn River Group and subsequently to the clay-rich Imperial Formation—they alone are not sufficient to extend detailed sequence stratigraphic interpretations from wells with extensive thin section coverage to those without. Here, the integration of three datasets (sedimentological, geochemical, and wireline) allowed for the resolution of sequence stratigraphic ambiguities and fine-scale correlation between localities. For example, depositional trends in the N-09 core revealed that a maximum regressive surface is present near the Canol–Imperial formational contact, which is not evident solely based on trends in wireline or geochemical proxies. Moreover, the inclusion of geochemical results enabled the identification of stratigraphic trends and signatures associated with fluctuations in detrital sediment abundance, biogenic Si, and paleoredox, facilitating the correlation of high-resolution sequences between study localities. For instance, this framework allows for the detailed identification and mapping of siliceous maximum flooding surfaces between the N-09 core and other wells of the Central Mackenzie Valley

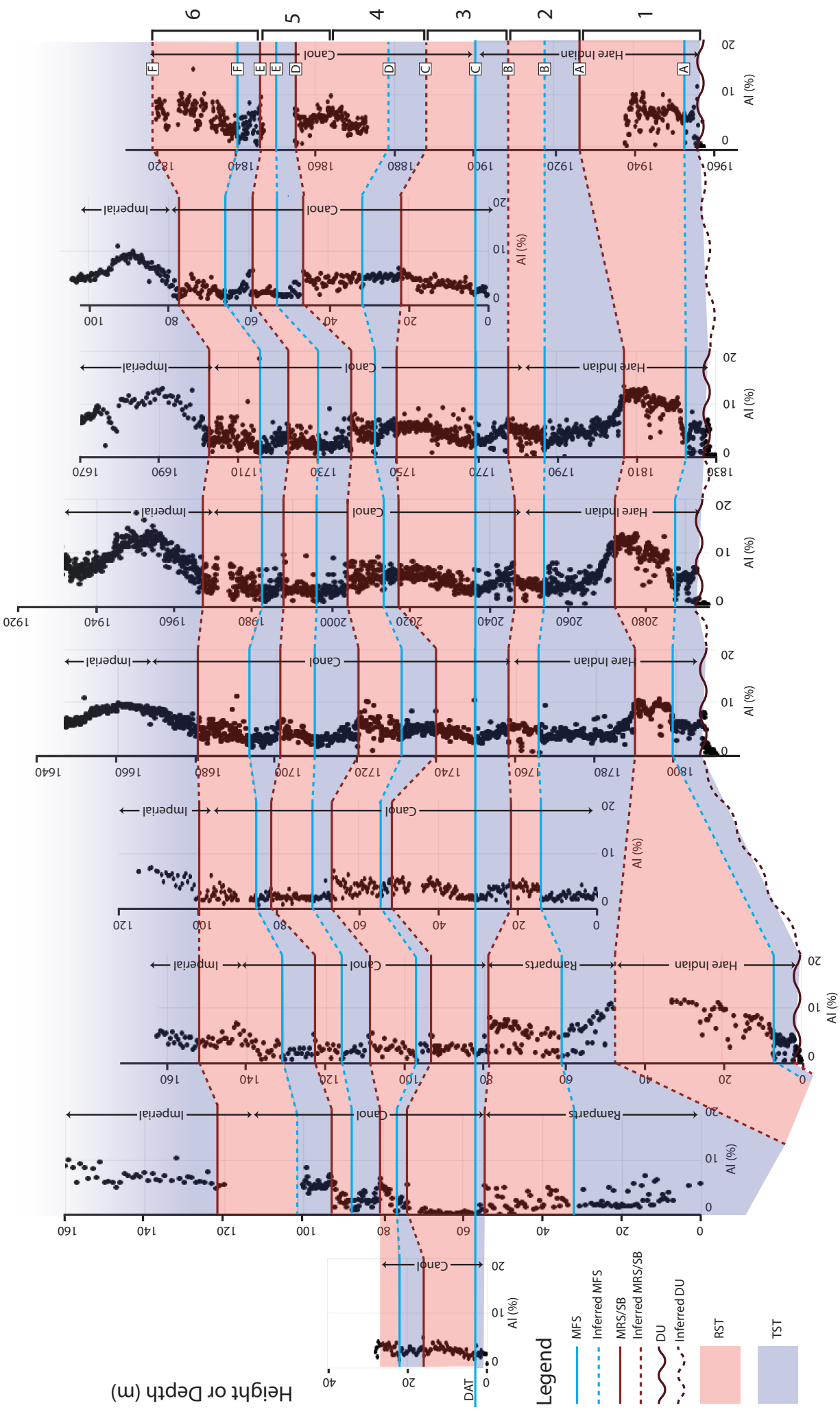

Figure 15 | Sequence stratigraphic correlation of the Horn River Group (Hare Indian, Canol, and Ramparts Formations) and lower Imperial Formation from outcrops in the Mackenzie Mountains and cores from the Central Mackenzie Valley, showing Al profiles in wt. %. Transgressive–regressive (T–R) sequences are numbered on the right side of the figure. Outcrop abbreviations: CR – Carcajou River, DC – Dodo Creek, MR – Mountain River, PC – Powell Creek, and RC – Rumbly Creek. Other acronyms and abbreviations: DAT – datum, DU – drowning unconformity, MFS – maximum flooding surface, MRS – maximum regressive surface, RST – regressive systems tract, SB – sequence boundary, and TST – transgressive systems tract.

5.6. Environmental forcing mechanisms

Both local and global environmental factors may have shaped compositional shifts across stratigraphic surfaces and systems tracts of the Horn River Group. Firstly, cycles in the proportion of detrital sediment—as suggested by fluctuations in the abundance of Al—would have been influenced by the balance between terrigenous sediment supply and relative sea level change. Along the Arctic margin of Laurentia, the Middle to Late Devonian was characterized by convergence and episodic terrane accretion (Anfinson et al., 2013; Hadlari et al., 2014; van Staal & Zagorevski, 2023), likely producing pulses of enhanced terrigenous sediment supply reaching the study area from the northern source region.

Secondly, fluctuations in relative sea level represent another important control on detrital sediment abundance, and these variations may be the result of global (eustatic) sea level variations, local tectonic activity, or a combination of both. A eustatic sea level curve for the Devonian was first proposed by Johnson et al. (1985) based on age-equivalent lithofacies cycles in strata of North America and Europe. This eustatic curve has since been updated by a number of studies (e.g., Becker et al., 2020; Haq & Schutter, 2008), and a review by Kabanov et al. (2023) calls into question the evidence for high-frequency (1 million-year or less) eustatic fluctuations in Middle to Late Devonian. Notably, there is no evidence for relative sea level fall in the Horn River Group strata included herein, or in Ramparts Formation platform and reef carbonates at other locations in the Mackenzie Mountains and Central Mackenzie Valley (e.g., Muir, 1988; Yose et al., 2001). Accordingly, T–R sequences and Al abundance fluctuations in the Horn River Group may largely reflect cycles in terrigenous sediment supply amidst a background of relative sea level rise associated with passive margin subsidence. In this case, regressive systems tracts would have been the product of lower rates of relative sea level rise paired with elevated rates of terrigenous sediment supply, producing a seaward shift in depositional environments.

The stratigraphic distribution of biogenic Si also shows cycles corresponding to transgressive–regressive cycles in the Horn River Group of our study area. This pattern of biogenic Si enrichment at maximum flooding surfaces has been observed in other Devonian mudstones of North America (e.g., the Duvernay Formation of Alberta and the Woodford Shale of Oklahoma) and attributed to increased biological productivity or decreased clastic dilution (N. B. Harris et al., 2018; Turner et al., 2016). Interestingly, when the depths of the sequence stratigraphic surfaces in the N-20 and N-09 cores are compared with the $\delta^{13}C$ profiles from the same cores, spikes in $\delta^{13}C$—interpreted to reflect increased biological productivity—commonly correspond to maximum regressive surfaces rather than maximum flooding surfaces ($\delta^{13}C$ profiles for the N-09 and N-20 cores are presented and interpreted in LaGrange et al., 2023). The correspondence between maximum regressive surfaces and instances of higher biological productivity suggests that reduced clastic dilution may have been the primary cause of enhanced levels of biogenic Si at maximum flooding surfaces in the Horn River Group.

Enrichment factors of the trace metals Mo and V—interpreted to reflect changes in paleoredox—also vary alongside shifts in depositional environments and transgressive–regressive cycles in the Horn River Group, with the highest enrichment at or just above maximum flooding surfaces (e.g., Figure 5). In an unrestricted basin at a seafloor position above the oxygen minimum zone, transgression is expected to reduce bottom water oxygenation by shifting both the oxygen minimum zone and wave base landward (N. B. Harris et al., 2013; LaGrange et al., 2020).

Moreover, global variations in marine oxygenation likely influenced bottom water paleoredox during deposition of the Horn River Group. In the latest Eifelian to Late Frasnian of the Devonian Period, eleven global marine biotic events have been recognized, including the Kačák, Taghanic, Frasnes, Middlesex (punctata), Rhinestreet, and Kellwasser events, which are associated with positive $\delta^{13}C$ excursions (e.g., Becker et al., 2020). In tropical shallow marine settings, global biotic events resulted in extinctions and overturn of many species, including corals, stromatoporoids, trilobites, brachiopods, ostracods, and ammonoids (e.g., Copper, 2002; House, 1985; Walliser, 1996). The cause of these events is generally attributed to expanded marine anoxia on continental shelves, although underlying triggers are debated (e.g., Carmichael et al., 2019; Lu et al., 2021; Walliser, 1996; Zambito et al., 2012). Based on redox-sensitive trace metal enrichment, Kabanov (2019) identified four intervals in the Horn River Group, interpreted as anoxic horizons (approximately corresponding to maximum flooding surfaces A, C, E, and F in this paper). With conodont biostratigraphy, Kabanov and Jiang (2020) suggested that these horizons correlate with the Kačák, Frasnes, Middlesex (punctata), and Rhinestreet events, and showed that the Kellwasser event occurs after deposition of the Horn River Group and is thus not recorded in the strata considered herein. Although every maximum flooding surface interpreted in this study is associated with some degree of V and Mo enrichment (e.g., Figure 5), the magnitude varies. Higher enrichment is observed at maximum flooding surfaces A, C, E, and F, suggesting that reduced bottom water oxygenation from local maximum flooding events may have also corresponded to events of globally increased marine anoxia, producing higher magnitude trace metal enrichment relative to maximum flooding surfaces B and D.

6. Conclusions

Chemostratigraphic proxies and depositional trends were used to establish a high-resolution sequence stratigraphic framework for the Middle to Late Devonian Horn River

Group of the west central NWT (Canada), spanning four cores in the Central Mackenzie Valley and five outcrop locations in the Mackenzie Mountains. This framework suggests the presence of six T–R cycles from the latest Eifelian to the Frasnian along the northwestern shelf of Laurentia. Sedimentologically, there was no evidence for the correlative conformity or regressive surface of marine erosion, meaning that regressive strata likely constitute highstand systems tracts. These findings, combined with results from the time-equivalent platform and reef carbonates (Muir, 1988; Yose et al., 2001), suggest a continuous rise in relative sea level in the study area from the latest Eifelian to the Frasnian. The enrichments of redox-sensitive trace metals V and Mo exhibit trends relative to indicators for terrigenous sediment and biogenic silica. These trends suggest that the most reducing conditions in the bottom water and/or seafloor sediment occurred during or shortly after the maximum flooding surfaces, indicating a relationship between fluctuations in local paleoredox, sediment supply, and relative sea level.

Owing to the subtle lithological variations characteristic of the Horn River Group mudstone interval, microscale sedimentological observations from thin sections were required to make robust depositional interpretations for sequence stratigraphic analysis. Nonetheless, obtaining a thin section dataset with extensive vertical and lateral coverage was not feasible in the Horn River Group, as is the case for most mudstone successions of economic or paleoceanographic significance around the globe. This study shows that chemostratigraphy can extend a sedimentology-based sequence stratigraphic framework across a broad area, facilitating subsurface mapping of surfaces and systems tracts. In the N-09 core of the Horn River Group, maximum flooding surfaces and maximum regressive surfaces each have a consistent and characteristic chemostratigraphic signature, facilitating their identification in cores and outcrops with sparse or no thin section coverage. However, the maximum regressive surface marking the transition from the Canol Formation to the Imperial Formation (and the shift from passive margin to foreland basin) is associated with a markedly different geochemical signature than the other maximum regressive surfaces in the N-09 core. This exception to the typical maximum regressive chemostratigraphic signature illustrates the value of integrating both sedimentological and geochemical datasets for sequence stratigraphy in fine-grained strata.

Acknowledgements

We are grateful to Husky Energy (now Cenovus Energy) for kindly allowing access to the N-09 and I-78 cores and for sharing with us their wireline datasets from the N-09 and I-78 wells. We would like to thank Dr. John Duke for providing guidance related to X-ray fluorescence methods and for sharing with us the USGS Brush Creek (SBC-1) standard. These authors are also grateful to everyone who helped with the powdering of outcrop samples, including Skye Lybbert, Nicole Atienza, Rizal Ignacio, Marcus Kehler, Sheridan Sigstad, Adam Lariviere, and Daniel Baker. We also thank Devon Frayn for help with data collection, Dave Herbers for helpful discussions related to the Horn River Group and chemostratigraphy, and Jiahui Gao for assistance with retrieving wireline logs. Moreover, the manuscript was greatly improved following feedback from editors Dr. Stéphane Bodin and Dr. Abosede Abubakre, reviewer Dr. Dario Harazim, an anonymous reviewer, and copy editor Tom Dodd. We appreciate their interest and constructive comments. Finally, we are grateful for the project funding provided by the Northwest Territories Geological Survey.

A portion of the X-ray florescence data included in this work was reproduced from the article entitled "Chemostratigraphy as a tool for sequence stratigraphy in the Devonian Hare Indian Formation in the Mackenzie Mountains and Central Mackenzie Valley, Northwest Territories, Canada" by Brette S. Harris, Maya T. LaGrange, Sara K. Biddle, Tiffany L. Playter, Kathryn M. Fiess, and Murray K. Gingras, which was published in the Canadian Journal of Earth Sciences volume 59 (pages 29–45, doi: dx.doi.org/10.1139/cjes-2020-0198).

Author contribution

Maya T. LaGrange: Conceptualization, Investigation, Visualization, Writing - Original Draft, Brette S. Harris: Investigation, Writing - Review & Editing, Sara K. Biddle: Investigation, Writing - Review & Editing, Smriti Dhiman: Formal Analysis, Octavian Catuneanu: Writing - Review & Editing, Kurt O. Konhauser: Supervision, Writing - Review & Editing, Viktor Terlaky: Conceptualization, Writing - Review & Editing, Murray K. Gingras: Conceptualization, Supervision, Writing - Review & Editing

Data availability

Four appendix tables are associated with this study, labelled A to D.

Conflict of interest

The authors declare that they have no known competing financial interests or personal relationships that could have appeared to influence the work reported in this paper.

References

Adachi, M., Yamamoto, K., & Sugisaki, R. (1986). Hydrothermal chert and associated siliceous rocks from the northern Pacific their geological significance as indication of ocean ridge activity. Sedimentary Geology, 47(1), 125–148. https://doi.org/10.1016/0037-0738(86)90075-8

Algeo, T. J., & Liu, J. (2020). A re-assessment of elemental proxies for paleoredox analysis. Chemical Geology, 540, 119549. https://doi.org/10.1016/j.chemgeo.2020.119549

Algeo, T. J., & Lyons, T. W. (2006). Mo–total organic carbon covariation in modern anoxic marine environments: Implications for analysis of paleoredox and paleohydrographic conditions. Paleoceanography, 21(1), 2004PA001112. https://doi.org/10.1029/2004PA001112

Algeo, T. J., Schwark, L., & Hower, J. C. (2004). High-resolution geochemistry and sequence stratigraphy of the Hushpuckney Shale (Swope Formation, eastern Kansas): Implications for climato-environmental dynamics of the Late Pennsylvanian Midcontinent Seaway. Chemical Geology, 206(3), 259–288. https://doi.org/10.1016/j.chemgeo.2003.12.028

Anfinson, O. A., Leier, A. L., Dewing, K., Guest, B., Stockli, D. F., & Embry, A. F. (2013). Insights into the Phanerozoic tectonic evolution of the northern Laurentian margin: Detrital apatite and zircon (U–Th)/He ages from Devonian strata of the Franklinian Basin, Canadian Arctic Islands. Canadian Journal of Earth Sciences, 50(7), 761–768. https://doi.org/10.1139/cjes-2012-0177

Arsairai, B., Wannakomol, A., Feng, Q., & Chonglakmani, C. (2016). Paleoproductivity and paleoredox condition of the Huai Hin Lat Formation in northeastern Thailand. Journal of Earth Science, 27(3), 350–364. https://doi.org/10.1007/s12583-016-0666-8

Becker, R. T., Marshall, J. E. A., Da Silva, A.-C., Agterberg, F. P., Gradstein, F. M., & Ogg, J. G. (2020). Chapter 22—The Devonian Period. In F. M. Gradstein, J. G. Ogg, M. D. Schmitz, & G. M. Ogg (Eds.), Geologic Time Scale 2020 (pp. 733–810). Elsevier. https://doi.org/10.1016/B978-0-12-824360-2.00022-X

Beranek, L. P., Mortensen, J. K., Lane, L. S., Allen, T. L., Fraser, T. A., Hadlari, T., & Zantvoort, W. G. (2010). Detrital zircon geochronology of the western Ellesmerian clastic wedge, northwestern Canada: Insights on Arctic tectonics and the evolution of the northern Cordilleran miogeocline. GSA Bulletin, 122(11–12), 1899–1911. https://doi.org/10.1130/B30120.1

Biddle, S. K., LaGrange, M. T., Harris, B. S., Egenhoff, S., & Gingras, M. K. (2025). Current concepts in mudstone description and deposition: A synthesis for mudstone initiates. Sedimentologika, 3(1). https://doi.org/10.57035/journals/sdk.2025.e31.1621

Biddle, S. K., LaGrange, M. T., Harris, B. S., Fiess, K., Terlaky, V., & Gingras, M. K. (2021). A fine detail physico-chemical depositional model for Devonian organic-rich mudstones: A petrographic study of the Hare Indian and Canol Formations, Central Mackenzie Valley, Northwest Territories. Sedimentary Geology, 414, 105838. https://doi.org/10.1016/j.sedgeo.2020.105838

Brown, J. S. (1943). Suggested use of the word microfacies. Economic Geology, 38(4), 325. https://doi.org/10.2113/gsecongeo.38.4.325

Brumsack, H.-J. (2006). The trace metal content of recent organic carbon-rich sediments: Implications for Cretaceous black shale formation. Palaeogeography, Palaeoclimatology, Palaeoecology, 232(2), 344–361. https://doi.org/10.1016/j.palaeo.2005.05.011

Calvert, S. E., & Pedersen, T. F. (1993). Geochemistry of Recent oxic and anoxic marine sediments: Implications for the geological record. Marine Geology, 113(1), 67–88. https://doi.org/10.1016/0025-3227(93)90150-T

Carmichael, S. K., Waters, J. A., Königshof, P., Suttner, T. J., & Kido, E. (2019). Paleogeography and paleoenvironments of the Late Devonian Kellwasser event: A review of its sedimentological and geochemical expression. Global and Planetary Change, 183, 102984. https://doi.org/10.1016/j.gloplacha.2019.102984

Catuneanu, O. (2004). Retroarc foreland systems–evolution through time. Journal of African Earth Sciences, 38(3), 225–242. https://doi.org/10.1016/j.jafrearsci.2004.01.004

Catuneanu, O. (2019). Model-independent sequence stratigraphy. Earth-Science Reviews, 188, 312–388. https://doi.org/10.1016/j.earscirev.2018.09.017

Catuneanu, O. (2022). Principles of sequence stratigraphy (2nd ed.). Elsevier. https://doi.org/10.1016/C2009-0-19362-5

Cocks, L. R. M., & Torsvik, T. H. (2011). The Palaeozoic geography of Laurentia and western Laurussia: A stable craton with mobile margins. Earth-Science Reviews, 106(1), 1–51. https://doi.org/10.1016/j.earscirev.2011.01.007

Copper, P. (2002). Silurian and Devonian Reefs: 80 Million Years of Global Greenhouse Between Two Ice Ages. In W. Kiessling, E. Flügel, & J. Golonka (Eds.), Phanerozoic Reef Patterns (pp. 181–238). Special Publications of SEPM. https://doi.org/10.2110/pec.02.72

Crombez, V., Rohais, S., Euzen, T., Riquier, L., Baudin, F., & Hernandez-Bilbao, E. (2020). Trace metal elements as paleoenvironmental proxies: Why should we account for sedimentation rate variations? Geology, 48(8), 839–843. https://doi.org/10.1130/G47150.1

Davis, C., Pratt, L. M., Sliter, W. V., Mompart, L., & Murat, B. (1999). Factors influencing organic carbon and trace metal accumulation in the Upper Cretaceous La Luna Formation of the western Maracaibo Basin, Venezuela. In E. Barrera & C. C. Johnson, Evolution of the Cretaceous Ocean-Climate System. Geological Society of America. https://doi.org/10.1130/0-8137-2332-9.203

Dewing, K., Hadlari, T., Pearson, D. G., & Matthews, W. (2019). Early Ordovician to Early Devonian tectonic development of the northern margin of Laurentia, Canadian Arctic Islands. GSA Bulletin, 131(7–8), 1075–1094. https://doi.org/10.1130/B35017.1

Egenhoff, S. O., & Fishman, N. S. (2013). Traces In the Dark—Sedimentary Processes and Facies Gradients In the Upper Shale Member of the Upper Devonian–Lower Mississippian Bakken Formation, Williston Basin, North Dakota, U.S.A. Journal of Sedimentary Research, 83(9), 803–824. https://doi.org/10.2110/jsr.2013.60

Eide, E. A. (2005). Analytical Methods: Geochronological Techniques. In R. C. Selley, R. M. Cocks, & I. R. Plimer (Eds.), Encylopedia of Geology (pp. 77–91). Elsevier. https://doi.org/10.1016/B0-12-369396-9/00103-9

Embry, A. F., & Johannessen, E. P. (1992). T–R sequence stratigraphy, facies analysis and reservoir distribution in the uppermost Triassic–Lower Jurassic succession, western Sverdrup Basin, Arctic Canada. In T. O. Vorren, E. Bergsager, Ø. A. Dahl-Stamnes, E. Holter, B. Johansen, E. Lie, & T. B. Lund (Eds.), Arctic Geology and Petroleum Potential (Vol. 2, pp. 121–146). Elsevier. https://doi.org/10.1016/B978-0-444-88943-0.50013-7

Erickson, B. E., & Helz, G. R. (2000). Molybdenum(VI) speciation in sulfidic waters: Stability and lability of thiomolybdates. Geochimica et Cosmochimica Acta, 64(7), 1149–1158.

Garzione, C. N., Patchett, P. J., Ross, G. M., & Nelson, J. (1997). Provenance of Paleozoic sedimentary rocks in the Canadian Cordilleran miogeocline: A Nd isotopic study. Canadian Journal of Earth Sciences, 34(12), 1603–1618. https://doi.org/10.1139/e17-129

Hadlari, T., Davis, W. J., & Dewing, K. (2014). A pericratonic model for the Pearya terrane as an extension of the Franklinian margin of Laurentia, Canadian Arctic. Geological Society of

America Bulletin, 126(1–2), 182–200. https://doi.org/10.1130/B30843.1

Hadlari, T., Tylosky, S. A., Lemieux, Y., Zantvoort, W. G., & Catuneanu, O. (2009). Slope and Submarine Fan Turbidite Facies of the Upper Devonian Imperial Formation, Northern Mackenzie Mountains, NWT. Bulletin of Canadian Petroleum Geology, 57(2), 192–208. https://doi.org/10.2113/gscpgbull.57.2.192

Hammes, U., & Frébourg, G. (2012). Haynesville and Bossier mudrocks: A facies and sequence stratigraphic investigation, East Texas and Louisiana, USA. Marine and Petroleum Geology, 31(1), 8–26. https://doi.org/10.1016/j.marpetgeo.2011.10.001

Haq, B. U., & Schutter, S. R. (2008). A Chronology of Paleozoic Sea-Level Changes. Science, 322(5898), 64–68. https://doi.org/10.1126/science.1161648

Harris, B. S., LaGrange, M. T., Biddle, S. K., Playter, T. L., Fiess, K. M., & Gingras, M. K. (2021). Chemostratigraphy as a tool for sequence stratigraphy in the Devonian Hare Indian Formation in the Mackenzie Mountains and Central Mackenzie Valley, Northwest Territories, Canada. Canadian Journal of Earth Sciences, 99, 1–17. https://doi.org/10.1139/cjes-2020-0198

Harris, B. S. S. (2020). Chemostratigraphy and facies analysis of the Hare Indian Formation in the Mackenzie Mountains and Central Mackenzie Valley, Northwest Territories, Canada [PhD Thesis]. University of Alberta (Canada). https://doi.org/10.7939/r3-2t6z-n494

Harris, N. B., McMillan, J. M., Knapp, L. J., & Mastalerz, M. (2018). Organic matter accumulation in the Upper Devonian Duvernay Formation, Western Canada Sedimentary Basin, from sequence stratigraphic analysis and geochemical proxies. Sedimentary Geology, 376, 185–203. https://doi.org/10.1016/j.sedgeo.2018.09.004

Harris, N. B., Mnich, C. A., Selby, D., & Korn, D. (2013). Minor and trace element and Re–Os chemistry of the Upper Devonian Woodford Shale, Permian Basin, west Texas: Insights into metal abundance and basin processes. Chemical Geology, 356, 76–93. https://doi.org/10.1016/j.chemgeo.2013.07.018

Helland-Hansen, W., & Martinsen, O. J. (1996). Shoreline trajectories and sequences; description of variable depositional-dip scenarios. Journal of Sedimentary Research, 66(4), 670–688. https://doi.org/10.1306/D42683DD-2B26-11D7-8648000102C1865D

Helz, G. R., Miller, C. V., Charnock, J. M., Mosselmans, J. F. W., Pattrick, R. A. D., Garner, C. D., & Vaughan, D. J. (1996). Mechanism of molybdenum removal from the sea and its concentration in black shales: EXAFS evidence. Geochimica et Cosmochimica Acta, 60(19), 3631–3642. https://doi.org/10.1016/0016-7037(96)00195-0

House, M. R. (1985). Correlation of mid-Palaeozoic ammonoid evolutionary events with global sedimentary perturbations. Nature, 313(5997), 17–22. https://doi.org/10.1038/313017a0

Irwin, D. (2020). Geology of the Northwest Territories (NWT Open Report 2020-007). Government of the Northwest Territories. https://doi.org/10.46887/2020-007

Johnson, J. G., Klapper, G., & Sandberg, C. A. (1985). Devonian eustatic fluctuations in Euramerica. GSA Bulletin, 96(5), 567–587. https://doi.org/10.1130/0016-7606(1985)96%253C567:DEFIE%253E2.0.CO;2

Kabanov, P. (2019). Devonian (c. 388–375 Ma) Horn River Group of Mackenzie Platform (NW Canada) is an open-shelf succession recording oceanic anoxic events. Journal of the Geological Society, 176(1), 29–45. https://doi.org/10.1144/jgs2018-075

Kabanov, P., & Deblonde, C. (2019). Geological and geochemical data from Mackenzie Corridor. Part VIII: Middle-Upper Devonian lithostratigraphy, formation tops, and isopach maps in NTS areas 96 and 106, Northwest Territories and Yukon (Geological Survey of Canada Open File Report No. 8552; p. 39). https://doi.org/10.4095/314785

Kabanov, P., & Gouwy, S. A. (2017). The Devonian Horn River Group and the basal Imperial Formation of the central Mackenzie Plain, N.W.T., Canada: Multiproxy stratigraphic framework of a black shale basin. Canadian Journal of Earth Sciences, 54(4), 409–429. https://doi.org/10.1139/cjes-2016-0096

Kabanov, P., & Gouwy, S. A. (2020). The type section of the Canol Formation (Devonian black shale) at Powell Creek: Critical assessment and correlation in the northern Cordillera, NWT, Canada. Bulletin of Canadian Petroleum Geology, 68(4), 123–140. https://doi.org/10.35767/gscpgbull.68.4.123

Kabanov, P., Hauck, T. E., Gouwy, S. A., Grasby, S. E., & van der Boon, A. (2023). Oceanic anoxic events, photic-zone euxinia, and controversy of sea-level fluctuations during the Middle-Late Devonian. Earth-Science Reviews, 241, 104415. https://doi.org/10.1016/j.earscirev.2023.104415

Kabanov, P., & Jiang, C. (2020). Photic-zone euxinia and anoxic events in a Middle-Late Devonian shelfal sea of Panthalassan continental margin, NW Canada: Changing paradigm of Devonian ocean and sea level fluctuations. Global and Planetary Change, 188, 103153. https://doi.org/10.1016/j.gloplacha.2020.103153

Knapp, L. J., McMillan, J. M., & Harris, N. B. (2017). A depositional model for organic-rich Duvernay Formation mudstones. Sedimentary Geology, 347, 160–182. https://doi.org/10.1016/j.sedgeo.2016.11.012

LaGrange, M. T., Atienza, N. M. M., Biddle, S. K., Harris, B. S., Fiess, K. M., Terlaky, V., Konhauser, K. O., & Gingras, M. K. (2022). The nature, origin, and predictors of porosity in the Middle to Late Devonian Horn River Group of the Central Mackenzie Valley, Northwest Territories, Canada. Marine and Petroleum Geology, 142, 105738. https://doi.org/10.1016/j.marpetgeo.2022.105738

LaGrange, M. T., Konhauser, K. O., Catuneanu, O., Harris, B. S., Playter, T. L., & Gingras, M. K. (2020). Sequence stratigraphy in organic-rich marine mudstone successions using chemostratigraphic datasets. Earth-Science Reviews, 203, 103137. https://doi.org/10.1016/j.earscirev.2020.103137

LaGrange, M. T., Li, K., Li, L., Kabanov, P., Konhauser, K. O., Harris, B. S., Biddle, S. K., Terlaky, V., & Gingras, M. K. (2023). An example of the Middle to Late Devonian marine nitrogen cycle from mudstones of the Horn River Group, Northwest Territories, Canada. Palaeogeography, Palaeoclimatology, Palaeoecology, 618, 111512. https://doi.org/10.1016/j.palaeo.2023.111512

Lazar, O. R., Bohacs, K. M., Macquaker, J. H. S., Schieber, J., & Demko, T. M. (2015). Capturing key attributes of fine-grained sedimentary rocks in outcrops, cores, and thin sections: Nomenclature and description guidelines. Journal of Sedimentary Research, 85(3), 230–246. https://doi.org/10.2110/jsr.2015.11

Li, C., Zhang, J., Li, W., Botting, J., Chen, Q., Fan, J., & Zhang, Y. (2021). Multiple glacio-eustatic cycles and associated environmental changes through the Hirnantian (Late Ordovician) in South China. Global and Planetary Change, 207, 103668. https://doi.org/10.1016/j.gloplacha.2021.103668

Lu, M., Lu, Y., Ikejiri, T., Sun, D., Carroll, R., Blair, E. H., Algeo, T. J., & Sun, Y. (2021). Periodic oceanic euxinia and terrestrial

fluxes linked to astronomical forcing during the Late Devonian Frasnian–Famennian mass extinction. Earth and Planetary Science Letters, 562, 116839. https://doi.org/10.1016/j.epsl.2021.116839

Mackenzie, W. S. (1970). Allochthonous Ree-Debris Limestone Turbidites Powell Creek, Northwest Territories. Bulletin of Canadian Petroleum Geology, 18(4), 474–492. https://doi.org/10.35767/gscpgbull.18.4.474

Macquaker, J. H. S., Taylor, K. G., & Gawthorpe, R. L. (2007). High-Resolution Facies Analyses of Mudstones: Implications for Paleoenvironmental and Sequence Stratigraphic Interpretations of Offshore Ancient Mud-Dominated Successions. Journal of Sedimentary Research, 77(4), 324–339. https://doi.org/10.2110/jsr.2007.029

Mazzotti, S., & Hyndman, R. D. (2002). Yakutat collision and strain transfer across the northern Canadian Cordillera. Geology, 30(6), 495–498. https://doi.org/10.1130/0091-7613(2002)030%3C0495:YCASTA%3E2.0.CO;2

Milad, B., Slatt, R., & Fuge, Z. (2020). Lithology, stratigraphy, chemostratigraphy, and depositional environment of the Mississippian Sycamore rock in the SCOOP and STACK area, Oklahoma, USA: Field, lab, and machine learning studies on outcrops and subsurface wells. Marine and Petroleum Geology, 115, 104278. https://doi.org/10.1016/j.marpetgeo.2020.104278

Morrow, D. W. (2018). Devonian of the Northern Canadian Mainland Sedimentary Basin: A Review. Bulletin of Canadian Petroleum Geology, 66(3), 623–694.

Muir, I. (1988). Devonian Hare Indian and Ramparts formations, MacKenzie Mountains, N.W.T. basin-fill, platform and reef development. [Thesis, University of Ottawa (Canada)]. https://doi.org/10.20381/ruor-10585

Muir, I., & Dixon, O. A. (1984). Facies analysis of a Middle Devonian sequence in the Mountain River-Gayna River. In J. Brophy (Ed.), Contributions to the geology of the Northwest Territories. (Vol. 1, pp. 55–62). Department of Indian Affairs and Northern Development, Canada.

Muir, I., Wong, P., & Wendte, J. (1985). Devonian Hare Indian-Ramparts (Kee Scarp) evolution, Mackenzie Mountains and subsurface Norman Wells, NWT: basin-fill and platform reef development. In M. W. Longman, K. W. Shanley, R. F. Lindsay, & D. E. Eby (Eds.), Rocky Mountain Carbonate Reservoirs: A Core Workshop (pp. 311–341). SEPM (Society for Sedimentary Geology). https://doi.org/10.2110/cor.85.07

Munsell Color. (2009). Geological rock-color chart: With genuine Munsell color chips. Munsell Color.

Pearce, T. J., Besly, B. M., Wray, D. S., & Wright, D. K. (1999). Chemostratigraphy: A method to improve interwell correlation in barren sequences — a case study using onshore Duckmantian/Stephanian sequences (West Midlands, U.K.). Sedimentary Geology, 124(1–4), 197–220. https://doi.org/10.1016/S0037-0738(98)00128-6

Pearce, T. J., Wray, D. S., Ratcliffe, K. T., Wright, D. K., Moscariello, A., Collinson, J. D., Evans, D. J., Holliday, D. W., & Jones, N. S. (2005). Chemostratigraphy of the upper Carboniferous Schooner Formation, southern North Sea. Carboniferous Hydrocarbon Geology: The Southern North Sea and Surrounding Onshore Areas: Yorkshire Geological Society, Occasional Publications Series, 7, 147–164.

Pellegrini, C., Sammartino, I., Schieber, J., Tesi, T., Paladini de Mendoza, F., Rossi, V., Chiggiato, J., Schroeder, K., Gallerani, A., Langone, L., Trincardi, F., & Amorosi, A. (2023). On depositional processes governing along-strike facies variations of fine-grained deposits: Unlocking the Little Ice Age subaqueous clinothems on the Adriatic shelf. Sedimentology, n/a(n/a). https://doi.org/10.1111/sed.13162

Plint, A. G. (2014). Mud dispersal across a Cretaceous prodelta: Storm-generated, wave-enhanced sediment gravity flows inferred from mudstone microtexture and microfacies. Sedimentology, 61(3), 609–647. https://doi.org/10.1111/sed.12068

Plint, A. G., & Nummedal, D. (2000). The falling stage systems tract: Recognition and importance in sequence stratigraphic analysis. Geological Society, London, Special Publications, 172, 1–17. https://doi.org/10.1144/GSL.SP.2000.172.01.01

Posamentier, H. W., & Allen, G. P. (1999). Siliciclastic Sequence Stratigraphy—Concepts and Applications (Vol. 7). SEPM Society for Sedimentary Geology. https://doi.org/10.2110/csp.99.07

Potma, K., Jonk, R., & Bohacs, K. M. (2022). Canol Formation, Northwest Territories, Canada—An Outcrop-to-Subsurface Analog for the Paleozoic Horn River Shale-gas Play. In K. M. Bohacs & O. R. Lazar (Eds.), Sequence stratigraphy: Applications to fine-grained rocks: AAPG Memoir 126 (pp. 295–344).

Potter, P. E., Maynard, J. B., & Depetris, P. J. (Eds.). (2005). Mud and Mudstones: Introduction and Overview. In Mud and Mudstones (pp. 1–6). Springer. https://doi.org/10.1007/3-540-27082-5_1

Powell, J. W., Issler, D. R., Schneider, D. A., Fallas, K. M., & Stockli, D. F. (2020). Thermal history of the Mackenzie Plain, Northwest Territories, Canada: Insights from low-temperature thermochronology of the Devonian Imperial Formation. GSA Bulletin, 132(3–4), 767–783. https://doi.org/10.1130/B35089.1

Pugh, D. C. (1983). Pre-Mesozoic geology in the subsurface of Peel River map area, Yukon Territory and district of Mackenzie (Memoir No. 401; p. 401). Geological Survey of Canada. https://doi.org/10.4095/119498

Pyle, L. J., & Gal, L. P. (2016). Reference Section for the Horn River Group and Definition of the Bell Creek Member, Hare Indian Formation in central Northwest Territories. Bulletin of Canadian Petroleum Geology, 64(1), 67–98. https://doi.org/10.2113/gscpgbull.64.1.67

Ratcliffe, K. T., Woods, J., & Rice, C. (2012). Determining Well-Bore Pathways during Multilateral Drilling Campaigns in Shale Resource Plays: An Example Using Chemostratigraphy from the Horn River Formation, British Columbia, Canada. Eastern Australasian Basin Symposium IV, Brisbane, Australia. https://archives.datapages.com/data/petroleum-exploration-society-of-australia/conferences/004/004001/pdfs/28.htm

Ratcliffe, K. T., Wright, A. M., & Schmidt, K. (2012). Application of inorganic whole-rock geochemistry to shale resource plays: An example from the Eagle Ford Shale Formation, Texas. The Sedimentary Record, 10(2), 4–9. https://doi.org/10.2110/sedred.2012.2.4

Sageman, B. B., & Lyons, T. W. (2003). Geochemistry of Fine-grained Sediments and Sedimentary Rocks. Treatise on Geochemistry, 7, 407. https://doi.org/10.1016/B0-08-043751-6/07157-7

Sano, J. L., Ratcliffe, K. T., & Spain, D. R. (2013). Chapter 7: Chemostratigraphy of the Haynesville Shale. In U. Hammes & J. Gales (Eds.), Geology of the Hanyesville Gas Shale in East Texas and West Louisiana, U.S.A. (pp. 137–154). AAPG Special Volumes. http://archives.datapages.com/data/specpubs/memoir105/data/137_aapg-sp1950137.htm

Schieber, J., & Zimmerle, W. (1998). The History and Promise of Shale Research. In J. Schieber, W. Zimmerle, & P. Sethi (Eds.), Shales and Mudstones (vol. 1): Basin Studies, Sedimentology and Paleontology (pp. 1–10). Schweizerbart'sche Verlagsbuchhandlung.

Scotese, C. R., & McKerrow, W. S. (1990). Revised World maps and introduction. Geological Society, London, Memoirs, 12(1), 1–21. https://doi.org/10.1144/GSL.MEM.1990.012.01.01

Scott, C., & Lyons, T. W. (2012). Contrasting molybdenum cycling and isotopic properties in euxinic versus non-euxinic sediments and sedimentary rocks: Refining the paleoproxies. Chemical Geology, 324–325, 19–27. https://doi.org/10.1016/j.chemgeo.2012.05.012

Scott, C., Slack, J. F., & Kelley, K. D. (2017). The hyper-enrichment of V and Zn in black shales of the Late Devonian-Early Mississippian Bakken Formation (USA). Chemical Geology, 452, 24–33. https://doi.org/10.1016/j.chemgeo.2017.01.026

Slatt, R. M., & Rodriguez, N. D. (2012). Comparative sequence stratigraphy and organic geochemistry of gas shales: Commonality or coincidence? Journal of Natural Gas Science and Engineering, 8, 68–84. https://doi.org/10.1016/j.jngse.2012.01.008

Tassonyi, E. J. (1969). Subsurface geology, lower Mackenzie River and Anderson River area, District of Mackenzie (Paper Nos. 68–25; p. 331). Geological Survey of Canada.

Taylor, S. R., & McLennan, S. M. (1985). The continental crust; its composition and evolution; an examination of the geochemical record preserved in sedimentary rocks. Blackwell.

Thöle, H., Bornemann, A., Heimhofer, U., Luppold, F. W., Blumenberg, M., Dohrmann, R., & Erbacher, J. (2020). Using high-resolution XRF analyses as a sequence stratigraphic tool in a mudstone-dominated succession (Early Cretaceous, Lower Saxony Basin, Northern Germany). The Depositional Record, 6(1), 236–258. https://doi.org/10.1002/dep2.83

Tribovillard, N., Algeo, T. J., Lyons, T., & Riboulleau, A. (2006). Trace metals as paleoredox and paleoproductivity proxies: An update. Chemical Geology, 232(1), 12–32. https://doi.org/10.1016/j.chemgeo.2006.02.012

Turner, B. W., Tréanton, J. A., & Slatt, R. M. (2016). The use of chemostratigraphy to refine ambiguous sequence stratigraphic correlations in marine mudrocks. An example from the Woodford Shale, Oklahoma, USA. Journal of the Geological Society, 173(5), 854–868. https://doi.org/10.1144/jgs2015-125

Van der Weijden, C. H. (2002). Pitfalls of normalization of marine geochemical data using a common divisor. Marine Geology, 184(3), 167–187. https://doi.org/10.1016/S0025-3227(01)00297-3

van Staal, C. R., & Zagorevski, A. (2023). Paleozoic tectonic evolution of the rifted margins of Laurentia. In S. J. Whitmeyer, M. L. Williams, D. A. Kellett, & B. Tikoff (Eds.), Laurentia: Turning Points in the Evolution of a Continent (Vol. 220, p. 0). Geological Society of America. https://doi.org/10.1130/2022.1220(24)

Ver Straeten, C. A., Brett, C. E., & Sageman, B. B. (2011). Mudrock sequence stratigraphy: A multi-proxy (sedimentological, paleobiological and geochemical) approach, Devonian Appalachian Basin. Palaeogeography, Palaeoclimatology, Palaeoecology, 304(1–2), 54–73. https://doi.org/10.1016/j.palaeo.2010.10.010

Walliser, O. H. (1996). Global Events in the Devonian and Carboniferous. In O. H. Walliser (Ed.), Global Events and Event Stratigraphy in the Phanerozoic (pp. 225–250). Springer Berlin Heidelberg.

Wang, Q., Huang, Y., Zhang, Z., Wang, C., & Li, X. (2022). Application of Chemical Sequence Stratigraphy to the Prediction of Shale Gas Sweet Spots in the Wufeng and Lower Longmaxi Formations within the Upper Yangtze Region. Minerals, 12(7), 859. https://doi.org/10.3390/min12070859

Wanty, R. B., & Goldhaber, M. B. (1992). Thermodynamics and kinetics of reactions involving vanadium in natural systems: Accumulation of vanadium in sedimentary rocks. Geochimica et Cosmochimica Acta, 56(4), 1471–1483. https://doi.org/10.1016/0016-7037(92)90217-7

Wehausen, R., & Brumsack, H.-J. (1999). Cyclic variations in the chemical composition of eastern Mediterranean Pliocene sediments: A key for understanding sapropel formation. Marine Geology, 153(1), 161–176. https://doi.org/10.1016/S0025-3227(98)00083-8

Wei, W., & Algeo, T. J. (2020). Elemental proxies for paleosalinity analysis of ancient shales and mudrocks. Geochimica et Cosmochimica Acta, 287, 341–366. https://doi.org/10.1016/j.gca.2019.06.034

Wesenlund, F., Grundvåg, S., Engelschiøn, V. S., Thießen, O., & Pedersen, J. H. (2022). Multi-elemental chemostratigraphy of Triassic mudstones in eastern Svalbard: Implications for source rock formation in front of the World's largest delta plain. The Depositional Record, 8(2), 718–753. https://doi.org/10.1002/dep2.182

Yose, L. A., Brown, S., Davis, T. L., Eiben, T., Kompanik, G. S., & Maxwell, S. R. (2001). 3-D geologic model of a fractured carbonate reservoir, Norman Wells Field, NWT, Canada. Bulletin of Canadian Petroleum Geology, 49(1), 86–116. https://doi.org/10.2113/49.1.86

Zambito, J. J., Brett, C. E., & Baird, G. C. (2012). The Late Middle Devonian (Givetian) Global Taghanic Biocrisis in Its Type Area (Northern Appalachian Basin): Geologically Rapid Faunal Transitions Driven by Global and Local Environmental Changes. In J. A. Talent (Ed.), Earth and life: Global biodiversity, extinction intervals and biogeographic perturbations through time. Springer Netherlands.

How to cite: LaGrange, M. T., Harris, B. S., Biddle, S. K., Dhiman, S., Catuneanu, O., Konhauser, K. O., Terlaky, V., & Gingras, M. K. (2025). Integrating chemostratigraphy and sedimentology for sequence stratigraphy in an enigmatic Middle to Late Devonian mudstone. Sedimentologika, 3(1), 1-28. https://doi.org/10.57035/journals/sdk.2025.e31.1695